國立交通大學

電子工程學系電子研究所

碩 士 論 文

螺旋式電感之物理模型

A Closed-Form Integral Model of Spiral Inductor
Using the Kramers–Kronig Relations

研 究 生：陳健章

指導教授：鄭裕庭　教授

中 華 民 國 九 十 五 年 六 月

螺旋式電感之物理模型

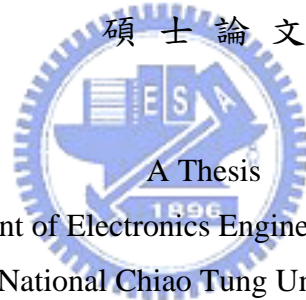# A Closed-Form Integral Model of Spiral Inductor
Using the Kramers–Kronig Relations

研 究 生：陳健章 　　　　　　　Student：Chien-Chang Chen

指導教授：鄭裕庭 　　　　　　　Advisor：Yu-Ting Cheng

國 立 交 通 大 學
電子工程學系電子研究所
碩 士 論 文

A Thesis
Submitted to Department of Electronics Engineering & Institute of Electronics
National Chiao Tung University
in Fulfillment of the Requirements
for the Degree of
Master
in

Electronics Engineering

June 2006

Hsinchu, Taiwan, Republic of China

中華民國九十五年六月

螺旋式電感之物理模型

學生：陳健章　　　　　　　　　　　　　　指導教授：鄭裕庭教授

國立交通大學電子工程學系電子研究所碩士班

摘　　　要

　　由於工業技術水準的提升以及人類生活的需求，便於攜帶的無線通訊系統被傾向於整合在高效能的電子元件上。射頻積體電路元件之特性亦被完整的研究與分析。特別是晶片螺旋式電感，其將扮演著射頻積體電路分析上最重要的角色。為了提升射頻積體電路之效率與實用性，此篇論文將提供一套新穎且簡單的物理方法以精準地分析、估計射頻晶片螺旋式電感之感值與共振頻率。有別於以往計算螺旋式電感感值的方法與侷限度，當改變電感的材料參數時，根據 Kramers-Kronig relations、電磁場論以及固態物理所推導而成之物理公式，本論文所提供之電感模型將可以協助尋求最佳的電感感值與共振頻率。更進一步地，本論文亦為提供計算螺旋式電感之共振頻率方法的先驅者。共振頻率的決定將可以協助電路分析人員以及微波工程師去選擇最為適當的電感頻寬。因此，本論文將提供了一套便利且精準的方法以輕易地解決設計層面的問題，並可以簡化且履行晶片射頻螺旋式電感在高頻積體電路的設計與應用。

A Closed-Form Integral Model of Spiral Inductor

Using the Kramers–Kronig Relations

Student：Chien-Chan Chen   Advisors：Dr. Yu-Ting Cheng

Department of Electronics Engineering

& Institute of Electronics

National Chiao Tung University

ABSTRACT

On-Chip spiral inductors have been developed and widely used for RFIC designs. Their relative characteristics including inductance, quality factor, self-resonant frequency, and loss mechanism….etc., have already been investigated in details. Especially, the prediction of inductance and self-resonant frequency of a spiral inductor will easily help circuit designers and microwave engineers to manufacture the RFICs. There are several methods to calculate inductance and self-resonant frequency of a spiral inductor, such as calculating circuit parameter, S-parameter, simulations utilizing computers, closed-form models, and measurement from experiments. The applied methods, however, are based only on the circuit designs parameters. Meanwhile, there are non-physical expressions. The physical meaningless factors in the circuit could not explain how to search out the optimum design based on a physical sense. All of these methods could not determine the self-resonant frequency and evaluate the inductance while altering the material of inductors. The computer

simulations could assist the engineers in circuit analysis, but it should spend great deal of hours to obtain the approximate results. Although this approach could precisely determine the self-resonant frequency, it is time-consuming in calculation and non-physically straightforward which could not help circuit designer to easily reach for an optimal design. Therefore, in order to surmount those predicaments this thesis will provide a physical method for predicting the inductance and self-resonant frequency of a spiral inductor.

序　　言

理論物理學家 Steven Weinberg 曾說：「我們都是化約主義者(reductionist)」，意指我們在普通物體內部的基本粒子中，都期待著能找到最深奧的解釋原理。雖然許多粒子物理學家都同意這個觀點，但是這套說法不盡然可以被世人完全接受。因為了解最底層的原理、最小最小尺度範圍的原理，與了解大自然其實是兩回事。雖然多少都可以**簡化**到基本粒子的範圍，但是人類在粒子迴旋加速器外頭的物理範疇的了解還僅是滄海之一粟。混沌的渦流、複雜系統內的大型結構、還有生命體本身，都是可以「從最簡單原理累積、疊加出來千變萬化、絢爛奪目的現象。」只是對於這些現象的解釋都還藏在方程式裡面，而我們還沒找到方法將其分離出來。

物理學家的模型就像地圖一樣，永遠不夠完備、不夠新穎，除非這張地圖可以成長到像它所代表的地區那麼大和那麼複雜。愛因斯坦把物理當做一個人會怎樣推想、組合手錶內部機件的一套觀念，比方說：那滴滴答答有節奏的聲響、指針按部就班的前進，他都可以想到一個好模型來解釋，只是誰也不敢說這個模型一定正確。愛因斯坦說：「他可以相信知識有個理想的極限存在，而人的心智正一步一步向這個極限邁進。因此我們便把這個極限稱為**客觀的真理**。」如此看來，愛因斯坦的時代似乎單純多了。在費曼(R. P. Feynman) 那個被稱作物理黃金歲月的時代裡知識永遠地增長，但是客觀的真理卻一步步退到迷霧中去了。量子力學帶來一個永遠解決不了的問題，卻也促使了物理學家在精神以及哲學層面有了進一步的思索與探討。畢竟，科學管不管用，就得看它能不能正確地預測事情。

當我在描繪、拼湊這張尚不完整亦不知去向的"地圖"時，我的指導教授鄭裕庭老師給了我長足且意境深遠的建議。雖然據稱由正統的物理學系畢業，但是我的思考模式卻如自我個性一般跳躍、不願規矩。若說我的思考邏輯如 D 調卡農般浮誇奔走、不知身在何處，那麼鄭裕庭老師的想法便如蕭邦的小狗圓舞曲般雖規矩地小踏步前進，卻也令人神遊嚮往、不住地向前尋芳。因此，許多精靈古怪卻又不迷失其本性的想法與成就便在我們兩人的著墨間誕生。細想跟隨著鄭老師的兩年半中，亦師亦友的他給了我莫大的自由而且支持我的自由，讓我由衷地深受感動。雖說「食君之祿、擔君之憂」，但我更因老師在經濟與學問上的付出與關懷而有泉湧以報之感。

Contents

Content

Chapter 6   Model Validation and Discussion

Figure Captions

Chapter 2

Chapter 3

Chapter 4

Chapter 1   Introduction

1.1 Overview

Integral passives are becoming increasingly important in realizing next generation electronics industry needs through gradual replacement of discrete. The need for integral passives emerges from the increasing consumer demand for product miniaturization thus requiring components must be reliable and controlled easily. The microelectronic industry has to respond the consumer demands in automotive. The last two decades have seen the development of personal computers, telecommunication, electronic equipment, devices and consumer sectors for product miniaturization with increasing functionality. In order to achieve the goal of miniaturization, the behaviors of miniaturized passive components must be realize clearly before fabrication. In addition, according to the National Electronics Manufacturing Initiative (NEMI), the integral passive is defined as the functional elements either embedded in or incorporated on the surface of an interconnecting substrate. Since the number of passive components may exceed both the number and the area of IC chips on a circuit board or a package, it is necessary to substantially estimate and predict the single performance and interaction between each other. Thus, the passive components potentially can offer the benefits of smaller size, more functionality, and better performance. As a result, it is necessary to develop a method to well predict the behavior of the passive components.

The microelectronic industry has to respond the consumer demands in automotive. The last two decades have seen the development of personal computers, telecommunication, electronic equipment, devices and consumer sectors for product with increasing functionality. Especially, the spiral inductors, one of the important passive components, have been properly developed and widely utilized for radio frequency integrated circuit (RFIC) designs. Their related characteristics, including inductance, quality factor, self-resonant frequency, and loss mechanism etc., have already been investigated in detail. A variety of methodologies to calculate the inductance of a spiral inductor, such as Greenhouse-based formulations [1]–[3],

empirical expressions [4], analysis and simulation of inductors and transformers in integrated circuits (ASITIC) [5], and several textbooks in physics and engineering, have been presented for the design applications.

Nevertheless, in order to facilitate the implementation of integrated inductors, a compact scalable physical model that can accurately predict the behaviors of the inductors with different technologies' parameters is still an important research topic for the RFIC design and optimization [4], [6]–[9]. Conventional inductor models [6]–[8] could calculate inductance precisely. The applied method, however, is based on the Greenhouse algorithm [1]. Though the algorithm is very accurate, it still employs numerous summation steps that depend on the number of interacting segments and overall combinations of parallel segments. Complicated geometrical analysis can not be avoided. Meanwhile, there are nonphysical expressions, obtained using a large number of fitting factors. Since the factors are created to overcome the imperfect of the fitting function, it is essential to create an accurate mathematical expression associated with the physical sense for the inductance calculation.

In this thesis, a closed-form integral model is presented for the rectangular, octagonal, and circular freely suspended micromachined spiral inductor. Based on the Kramers-Kronig relations, field theory, and solid state physics [10]–[12], the model can actually describe behaviors of the free electrons in metal to characterize a spiral inductor which RFIC designers could easily have the optimal design utilizing this analytical method. Meanwhile, this model can exactly predict the inductance and self-resonant frequency of the spiral inductor without complicated geometrical analysis. Simulation and measurement results have validated the accuracy of the model. Furthermore, unlike conventional formulations only based on circuit parameters, this model could safely predict the inductance and the self-resonant frequency when altering the material of a spiral inductor.

1.2 Thesis Organization

First, the Kramers-Kronig relations using for metal will be well defined in chapter 2. The causality principle is the main point over through the chapter. The symmetry of the susceptibility function will posed in the end. In chapter 3, the paramagnetic and diamagnetic factors will be evaluated according to the Pauli spin principle and Larmor theorem. The Kramers-Kronig relations will be modified in this chapter to describe the behavior of anomalous dispersion and resonant absorption while the self-resonant occurs in a metal. Considering the quantum effect and high free electron density in metals, the kinetic energy of free electrons will be posed. The wave number is a factor of the kinetic energy, so that we may modify this factor to identify the relation between the inductor length and electron wavelength when the inductor start resonating. The scattering field and energy stored in the corners of the inductor will be developed by means of the conception of Compton scattering effect. Therefore, combining the kinetic energy and the scattering energy, the self-resonant frequency of the rectangular, octagonal, and circular spiral inductor can be well predicted so as to match the conservation law.

Extracting the susceptibility function, magnetic factor, and self-resonant frequency in chapter 3 and employing the conception of the velocity distribution from Sommerfeld, the evaluation of inductance of rectangular and octagonal spiral inductor will be developed in chapter 4. Compared to the conventional methods, the model will show itself as powerful tool in prediction of the inductance. The ground pad issue will be independently discussed in chapter 5. Spherical Green's function and Dirichlet condition will be adopted to describe the behavior of fields between the spiral inductor and ground pad. The result poses the fact that the inductor can be seen as a freely system while the ground pad far from 60 μm [18] at least.

The final chapter addresses the model validation and discussion. The model is examined by comparing with the contemporary calculations, including the results derived from the Greenhouse-based model and Ansoft-HFSS simulator, respectively. Meanwhile, the accuracy of HFSS analysis will be experimentally validated. It will be shown that a good parameter

match between the measurement and HFSS simulation in a Smith chart. After all, the model calculation will show a good predictions of inductance compared to the simulation.

Chapter 2   The Kramers–Kronig Relations for Metals

2.1   Introduction

The Kramers-Kronig relations compose of one of the most elegant and general theorems in physics, because they depend on their validity only on the principle of causality: the response can not before the stimulation. Based simply on this principle, the Kramers-Kronig relations can describe the interdependence of the real and imaginary parts of the susceptibility $\chi(\omega)$. Thus, the Kramers-Kronig relations can explain in the most fundamental and general terms, completely independent of the underlying physical mechanisms, the intimate connection between refraction and absorption. In fact, given one, the other follows immediately. Before deriving the Kramers-Kronig relations established in the complex frequency (ω) domain plane, the constitutive relations in dispersive media have to be characterized first.

The origin of dispersion is to be found in the different time scales that characterize real media and make different phenomena at different frequencies. The response of the medium to the applied fields is not instantaneous because of the electrons and nuclei have finite mass. The polarization and magnetization of the medium at time t therefore depend on the entire histories $\vec{E}(t')$ and $\vec{H}(t')$ of the fields at the point in question, and this must be represented by the constitutive relations. In order to simplify the mathematical structure, the medium is assumed to be isotropic, linear, but dispersive. In this case, of course, the polarization and the magnetization are in the direction of the electric field and the magnetic field, respectively. Thus, the constitutive relations may be the form:

$$\vec{P}(t) = \varepsilon_0 \int_{-\infty}^{\infty} \vec{E}(t') G_e(t-t')dt' \tag{1}$$

$$\vec{M}(t) = \varepsilon_0 \int_{-\infty}^{\infty} \vec{H}(t') G_m(t-t')dt' \tag{2}$$

where $G_e(t-t')$ and $G_m(t-t')$ are called the response functions for the polarization and the magnetization, respectively. Physically, the response function describes the behavior of the

system as a function of the time t following a unit impulse at time t'. The principle of causality address that the polarization at time t can not depend on the electric field at later times $t'>t$. Therefore,

$$G(\tau)=0 \qquad \text{for } \tau<0 \tag{3}$$

for either the dielectric or the magnetic response function and $\tau=t-t'$ here.

It is convenient for many problems to change from the time domain to the frequency domain. By taking the Fourier transform of the constitutive relations (1) and (2) using the Faltung theorem, the forms become:

$$\widetilde{\vec{P}}(\omega)=\varepsilon_0\chi_e(\omega)\widetilde{\vec{E}}(\omega) \tag{4}$$

and

$$\widetilde{\vec{M}}(\omega)=\chi_m(\omega)\widetilde{\vec{H}}(\omega) \tag{5}$$

The function $\chi_e(\omega)$ and $\chi_m(\omega)$ are called the dielectric and magnetic susceptibilities. In terms of the response function $G(\tau)$, the susceptibility has the form

$$\chi(\omega)=\int_{-\infty}^{\infty}G(\tau)e^{i\omega\tau} \tag{6}$$

It is note that since the response function $G(\tau)$ is real, the susceptibility defined by equation (6) has the symmetry property

$$\chi(-\omega)=\chi^*(\omega^*) \tag{7}$$

This equation indicates the fact that symmetry of electromagnetic energy while energy absorption or transformation occurring in a metal.

2.2 *The Kramers-Kronig Relations for Metals*

The domain in the complex frequency plane in which the susceptibility function is analytic is established just by the principle of causality (3), completely independent of the physical mechanism causing the dispersion. Assuming, for the moment, that the response function $G(\tau)$ is absolutely integrable and has at most a finite number of finite discontinuities, so the Riemann-Lebesgue lemma assure that

$$\chi(\omega)\xrightarrow[|\omega|\to\infty]{}0 \tag{8}$$

In fact, conductors violate this assumption, and it will be dealt later. For now considering the integral $\oint \chi(\omega)e^{-i\omega\tau}d\omega$, the Fourier transform of causality, around a contour enclosing the upper half of the complex frequency plane, as shown in Figure 1. From Cauchy's residue theorem we know that

$$\oint \chi(\omega)e^{-i\omega\tau}d\omega = 2\pi i \sum_n \left[e^{-i\omega_n\tau} \times \text{residue of } \chi(\omega_n) \right] \tag{9}$$

where ω_n is the nth pole of the function $\chi(\omega)$ inside the contour. Provided that $\chi(\omega)$ has only a finite number of poles, we can make the radius R lager enough to enclose all the poles in the upper half plane. The contour integral consists of two parts, these being the integral along the real axis and the integral around the semicircle, so that

$$\lim_{R\to\infty}\oint \chi(\omega)e^{-i\omega\tau}d\omega = \int_{-\infty}^{\infty}\chi(\omega)e^{-i\omega\tau}d\omega + \lim_{R\to\infty}\int_R \chi(\omega)e^{-i\omega\tau}d\omega \tag{10}$$
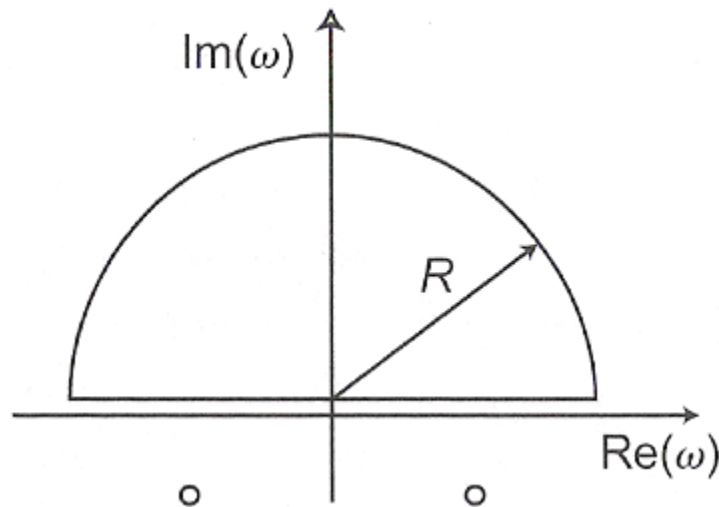
Fig. 1   Contour enclosing the upper half plane [10]

The first term of the right hand side is just the response function $G(\tau)$, which vanishes for $\tau < 0$ to satisfy the requirements of causality. The magnitude of the second integrand is

$$\left| \chi(\omega) e^{-i\omega\tau} \right| < \left| \chi(\omega) \right| e^{y\tau} \qquad (11)$$

where $\omega = x + iy$. Equation (11) vanishes exponentially above the real axis for $\tau < 0$, so the second term vanishes also. Combining the results discussed above the contour integral may be

$$\oint \chi(\omega) e^{-i\omega\tau} d\omega = 2\pi i \sum_n \left[e^{-i\omega_n\tau} \times \text{residue of } \chi(\omega_n) \right] = 0 \quad \text{for } \tau < 0 \qquad (12)$$

Therefore, there can be no poles of $\chi(\omega)$ in the upper half plane, while the response function satisfies the principle of causality.

Considering the function with simple pole $\chi(\omega)/(\omega - \omega_0)$, where ω_0 is a point on the real axis, as shown in Figure 2. If we integrate $\chi(\omega)/(\omega - \omega_0)$ around the upper plane using the contour shown in Figure 2, the result vanishes by Cauchy's theorem. But the contour is composed of several segments, and the form can be

$$\int_{-\infty}^{\omega_0-\varepsilon} \frac{\chi(\omega)}{\omega - \omega_0} d\omega + \int_{\omega_0+\varepsilon}^{\infty} \frac{\chi(\omega)}{\omega - \omega_0} d\omega + \int_{\varepsilon} \frac{\chi(\omega)}{\omega - \omega_0} d\omega + \lim_{R\to\infty} \int_R \frac{\chi(\omega)}{\omega - \omega_0} d\omega = 0 \qquad (13)$$

The last term vanishes in the limit $R \to \infty$, since $\chi(\omega)$ vanishes due to the Riemann-Lebesgue lemma. In the limit $\varepsilon \to 0$, the first two terms become the principal part of the integral form $-\infty$ to ∞. The third term, the integral along the semicircle around the pole at ω_0, can be evaluated from half the residue at the pole, so
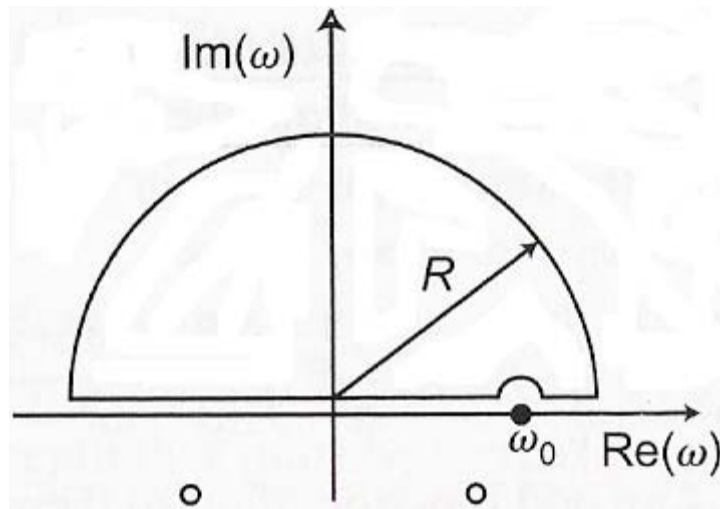
Fig. 2　　　Contour for deriving the Kramers-Kronig relations [10]

8

$$\lim_{\varepsilon \to 0} \int_{\varepsilon} \frac{\chi(\omega)}{\omega - \omega_0} d\omega = -\pi\, i \chi(\omega_0) \tag{14}$$

where the negative sign appears because the clockwise halfway around the pole is taking. Thus, the result can be obtained

$$\chi(\omega_0) = \frac{1}{\pi i} P \int_{-\infty}^{\infty} \frac{\chi(\omega)}{\omega - \omega_0} d\omega \tag{15}$$

where **P** stands for principal part. The importance of this remarkable equation follows from the appearance of i on the right hand side, for if separating the real and imaginary parts of equation (15), the relations can be getting as

$$\mathrm{Re}\,\chi(\omega_0) = \frac{1}{\pi} P \int_{-\infty}^{\infty} \frac{\mathrm{Im}\chi(\omega)}{\omega - \omega_0} d\omega \tag{16}$$

$$\mathrm{Im}\,\chi(\omega_0) = -\frac{1}{\pi} P \int_{-\infty}^{\infty} \frac{\mathrm{Re}\chi(\omega)}{\omega - \omega_0} d\omega \tag{17}$$

It is note that if the susceptibility has a real part then it necessarily has an imaginary part, and vice versa. Since dissipation is associated with the imaginary part of the susceptibility and dispersion with real part, we can not have one without the other.

These relations can be put in a more convenient form in the following way. If we multiply the integrand of equation (16) by $(\omega + \omega_0)/(\omega + \omega_0)$, then we get

$$\mathrm{Re}\,\chi(\omega_0) = \frac{1}{\pi} P \int_{-\infty}^{\infty} \frac{\omega\,\mathrm{Im}\chi(\omega)}{\omega^2 - \omega_0^2} d\omega + \frac{1}{\pi} P \int_{-\infty}^{\infty} \frac{\omega_0\,\mathrm{Im}\chi(\omega)}{\omega^2 - \omega_0^2} d\omega \tag{18}$$

From the equation (7) we see that $\mathrm{Im}\,\chi(\omega)$ is an odd function of ω, so the second term vanishes. Since the integrand in first term is even, we may write it as an integral over positive frequency only,

$$\mathrm{Re}\,\chi(\omega_0) = \frac{2}{\pi} P \int_{0}^{\infty} \frac{\omega\,\mathrm{Im}\chi(\omega)}{\omega^2 - \omega_0^2} d\omega \tag{19}$$

In the same way, we find that

$$\mathrm{Im}\,\chi(\omega_0) = -\frac{2}{\pi} P \int_{0}^{\infty} \frac{\omega_0\,\mathrm{Re}\chi(\omega)}{\omega^2 - \omega_0^2} d\omega \tag{20}$$

9

Note carefully that it is important to remember the symmetry of susceptibility functions. It is also the characteristics of conductors that the magnetic susceptibility $\chi_m(\omega)$ has a simple pole and a δ-function on the real axis at the origin. By employing the residues at the origin and the identities

$$\lim_{\omega \to 0}\left[\frac{1}{\omega - \omega_0}\right] = \lim_{\omega \to 0}\left[\frac{\omega_0}{\omega^2 - \omega_0^2} + i\frac{i\omega}{(i\omega)^2 + \omega_0^2}\right] \tag{21}$$

to evaluate the behavior of low frequency due to the singularity, the Kramers-Kronig relations can be modified as

$$\operatorname{Re}\chi(\omega_0) = \pi\sigma_0\delta(\omega_0) + \frac{2}{\pi}P\int_0^\infty \frac{\omega\operatorname{Im}\chi(\omega)}{\omega^2 - \omega_0^2}d\omega \tag{22}$$

$$\operatorname{Im}\chi(\omega_0) = \frac{\sigma_0}{\omega_0} - \frac{2}{\pi}P\int_0^\infty \frac{\omega_0\operatorname{Re}\chi(\omega)}{\omega^2 - \omega_0^2}d\omega \tag{23}$$

where σ_0 is the dc conductivity of metal. Therefore, the Kramers-Kronig relations for metals are presented.

Chapter 3 Determination of Self-resonant Frequency

3.1 Characteristics of Anomalous Dispersion and Resonant Absorption

The concurrence relationship of the real and image parts of the Kramers-Kronig relations are modified the form to explain certain characteristics in this section. For instance, preceded with the Lorentz–Drude Model (1900) in a conducting medium, a phenomenon called anomalous dispersion occurring near a narrow absorption feature, i.e., resonant absorption in a metal vapor, can be well represented in terms of the utilization of equation (22) and (23) to describe the relation between resonant absorption and anomalous dispersion as shown in Figure 3. The dispersion and absorption are coupled and associated with the real and imaginary parts of the susceptibility, respectively. If a medium has an imaginary component of the susceptibility at the self-resonant frequency, it must have a real component over a broad range of frequencies around the self-resonant frequency. While the resonance occurs, the energy of incident EM wave is fully absorbed by the free electrons inside the medium and the absorption is peaked strongly at the resonant frequency. Similar physical behavior of the resonance is also applicable for the case of a spiral inductor. The self-resonance occurrence of the spiral inductor would result in complete energy transformation from stored magnetic energy into electrical energy, and vice versa. The occurrence of the energy exchange is similar to the anomalous dispersion in which the incident EM wave is totally absorbed by the conducting medium and transformed into the kinetic energy and scattering potential of the free electrons. Therefore, we can construct a physic-based inductor model using the Kramers–Kronig relations. First, we assume that the inductor is perfect for EM wave signal propagation without having any energy loss. Thus, the imaginary part, (23), could be rationalized as a very narrow absorption of the EM wave at self-resonant frequency, ω_r, due to the energy transformation and it can be modified as

$$\operatorname{Im}\chi(\omega)=\frac{\sigma_0}{\omega}+\frac{\pi}{2}\frac{\alpha\delta(\omega-\omega_r)}{\omega_r} \tag{24}$$
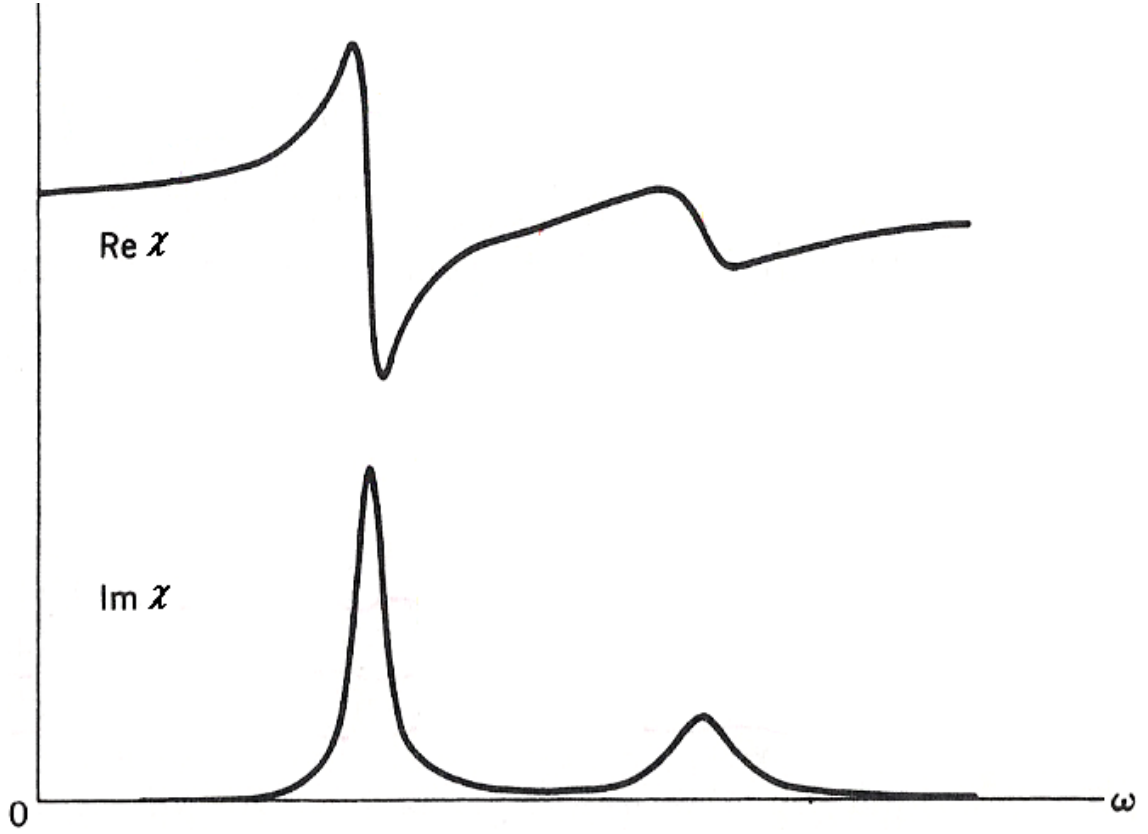
Fig. 3   Real and imaginary parts of the susceptibility function in the neighborhood of two resonances. The

region of anomalous dispersion is also the frequency interval where absorption occurs [11]

which accompanied with the real part as the following:

$$\mathrm{Re}\,\chi(\omega) \approx \frac{\sigma_0}{\pi}\left[\pi^2\delta(\omega) - \frac{\ln\omega}{\omega}\right] + \frac{\alpha}{\omega_r^2 - \omega^2} \tag{25}$$

where the magnetic factor α can be evaluated by employing the model of Pauli spin

paramagnetism at absolute temperature and Larmor theorem [12, 13]. In order to improve the

confusion in mathematics and approach the simplification in physics, a new definition of

susceptibility function must be presented to replace the conventional magnetic susceptibility

function:

$$\mu_0\left(1 + \chi_m\right) \rightarrow \mu_0\chi \tag{26}$$

For discussion in high frequency region, the new susceptibility function can be reduced as:

$$\mathrm{Re}\,\chi(\omega) \approx \frac{\alpha}{\omega_r^2 - \omega^2} \tag{27}$$

12

Thus, we can easily employ the equation (27) with new physical mission without complicated mathematical structure. The magnetic factor α can have more physical meanings.

Considering the free electron density (n_e) with magnetic moments parallel to the presented magnetic energy (μB), the form is

$$n_e^+ = \frac{1}{2}\int_{-\mu B}^{\hbar\omega_r} D(\varepsilon + \mu B)d\varepsilon \cong \frac{1}{2}\int_0^{\hbar\omega_r} D(\varepsilon)d\varepsilon + \frac{1}{2}\mu B D(\hbar\omega_r) \qquad (28)$$

where $\hbar$ is the Planck's constant. Here $\frac{1}{2}D(\varepsilon + \mu B)$ is the density of orbital of one spin orientation with energy $\varepsilon + \mu B$. The free electron density with magnetic moments antiparallel to the presented magnetic field is

$$n_e^- = \frac{1}{2}\int_{\mu B}^{\hbar\omega_r} D(\varepsilon - \mu B)d\varepsilon \cong \frac{1}{2}\int_0^{\hbar\omega_r} D(\varepsilon)d\varepsilon - \frac{1}{2}\mu B D(\hbar\omega_r) \qquad (29)$$

Figure 4 shows the Pauli paramagnetism at absolute zero. The schemes present the total energy of electrons with different spin direction relates to the density of orbital. Combining the equation (28) and (29), the paramagnetic factor, α_P, is given by

$$\alpha_P = \frac{\mu\omega_r^2}{B}\left(n_e^+ + n_e^-\right) = \mu^2\omega_r^2 D(\hbar\omega_r) = \mu^2\omega_r^2 \frac{3}{2}\frac{n_e}{\hbar\omega_r} = \frac{3n_e\mu^2\omega_r}{2\hbar} \qquad (30)$$

It is noted that the magnetic moment, μ, shall be carefully defined in this case. The energy levels of the system in a presented magnetic field are

$$U = -\vec{\mu}\cdot\vec{B} = m_J g\mu_B B \qquad (31)$$

where m_J is the azimuthal quantum number and has the values J, $J-1$,……, $-J$, factor g is the spectroscopic factor, and μ_B is the Bohr magneton. For a single spin with no orbital moment we have $m_J = \pm\frac{1}{2}$ and $g = 2$, whence $U = \pm\mu_B B$. Thus, the paramagnetic factor may be modified and has the form as

$$\alpha_P = \frac{3n_e\mu_B^2\omega_r}{2\hbar} \qquad (32)$$

13

Total energy, kinetic +
magnetic, of electrons

Fermi level

Parallel
to field

Opposite
to field

$2\mu B$

Density of
orbitals

Parallel
to field

Density of
orbitals

(a)   (b)
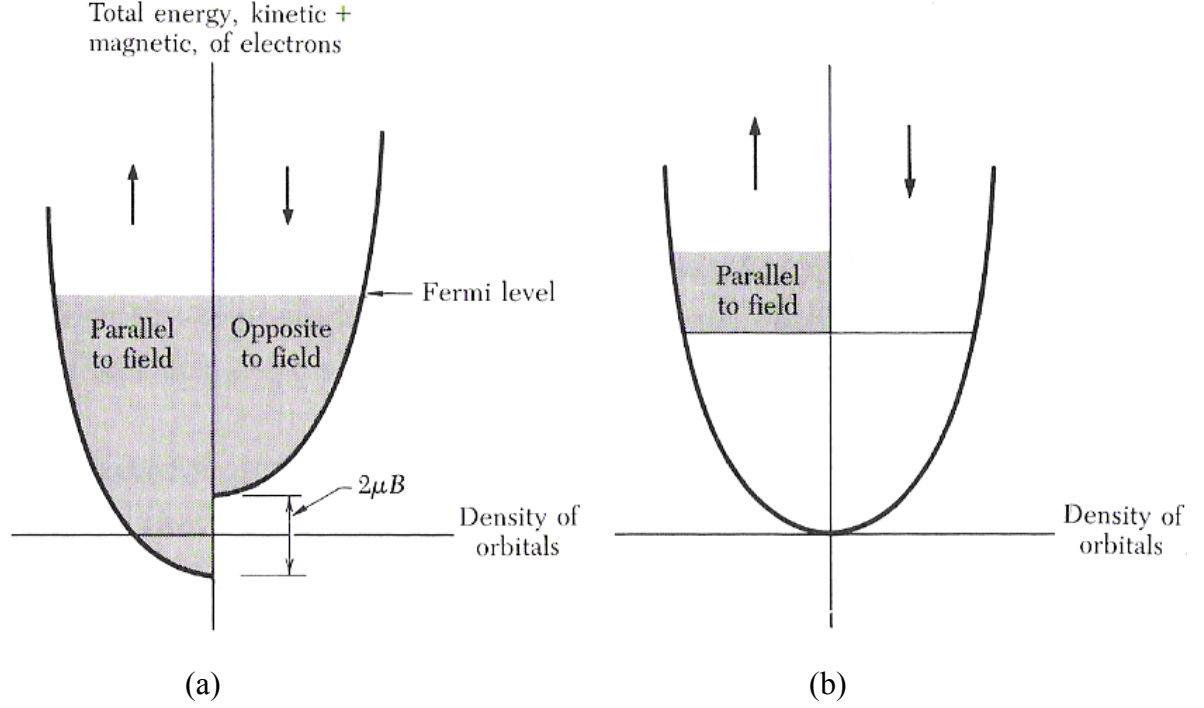
Fig. 4   Pauli paramagnetism at absolute zero. The orbitals in the shaded regions in (a) are occupied. The

numbers of electrons in the "up" and "down" band will adjust to make the energies equal at the Fermi

level. The chemical potential (Fermi level) of the moment up electrons is equal to that of the moment

down electrons. In (b) we show the excess of moment up electrons in magnetic field [12]

Analogous with the Larmor theorem, the diamagnetic factor of the system can be approximately calculated and the form is

$$\alpha_D = \frac{3n_e\mu\omega_r}{B} = \frac{3n_e\omega_r}{B}\left(-\frac{e^2B}{6m_e}\langle r^2 \rangle\right) = -\frac{e^2n_e\omega_r}{2m_e}\sum_{m=0}^{[n-1]}(l_{max} - 2ms)^2 \tag{33}$$

where the symbol [n-1] and m_e represent the Gaussian symbol where n is the number of turns and mass in material, respectively. The parameters, l_{max} and s, represent the maximum edge and line spacing of the inductor, respectively. Thus, by combining equation (32) and (33) the magnetic factor is

$$\alpha = \alpha_P + \alpha_D = \frac{3n_e\mu_B^2\omega_r}{2\hbar} - \frac{e^2n_e\omega_r}{2m_e}\sum_{m=0}^{[n-1]}(l_{max} - 2ms)^2 \tag{34}$$

For a spiral inductor with the geometry as shown in Figure 5, the material-depended magnetic factor may be modified via different material parameters and individual magnetic moments of the material.
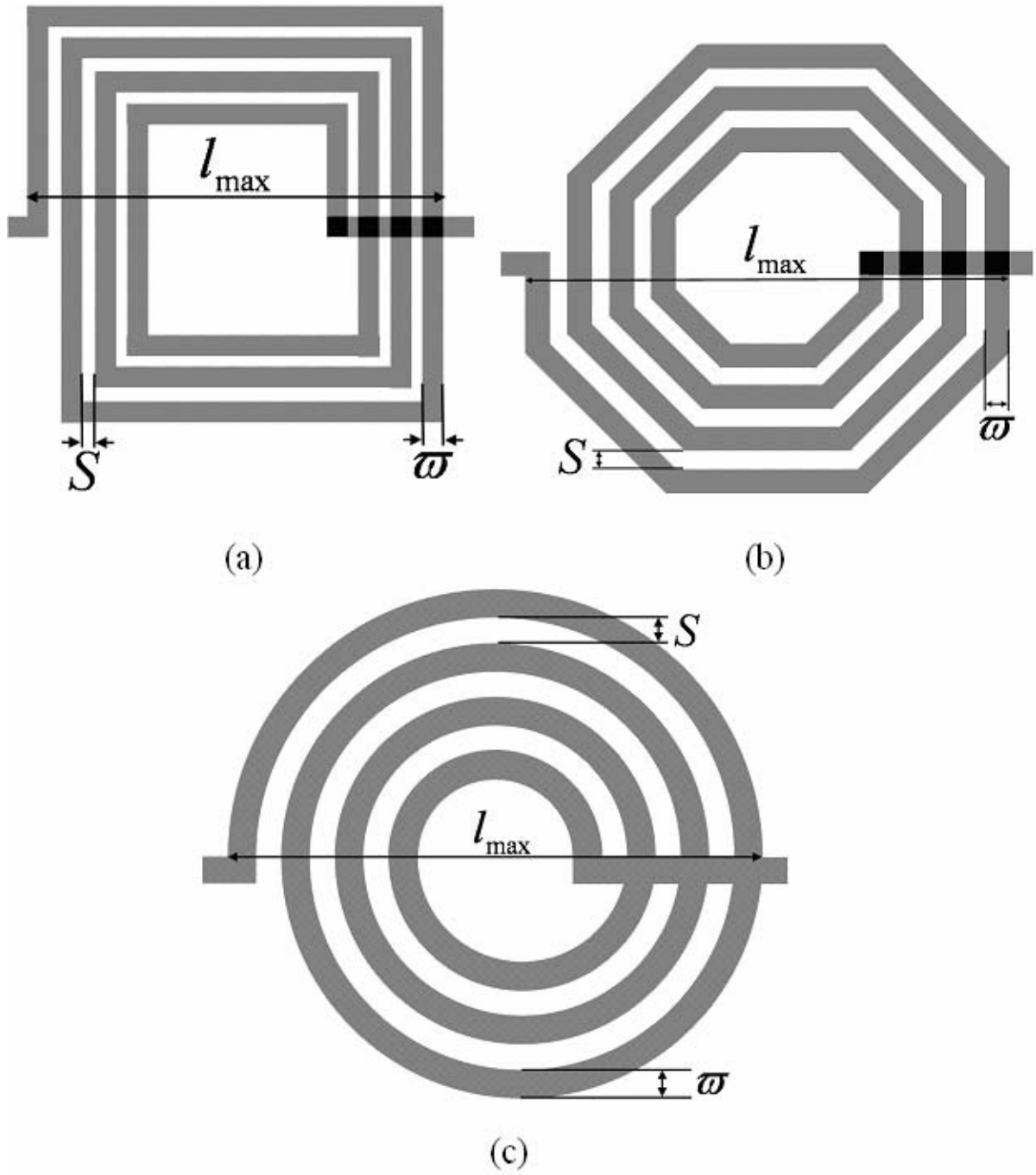
Fig. 5   Schematic diagram of the two-port spiral polygon inductor realizations: (a) rectangular, (b) octagonal, (c) circular. l_{max}, s, and ϖ are the maximum edge, line spacing, and line width of the polygon inductor, respectively

3.2 *Kinetic Energy of Free Electrons in Metal*

Looking for wavelike solution in which the vector potential **A** vanishes and the scalar potential Φ has the form of a plane wave. Thus, the transverse electric and magnetic fields vanish and only the longitudinal electric field remains. In this case the existence of a characteristic frequency, plasma frequency, for electrostatic oscillations should be discussed. The feature of the plasma frequency, however, is independence of wave number k and then the phase velocity can be any value. For the same reason, the group velocity will vanish. Therefore, aside from the effects of thermal motions, classical plasma waves do not propagate.

It is noted that the energy in the electric field is just equal to the electron kinetic energy when averaged over a cycle of the oscillation, in which the electrons and the field form a closed, conservative system. Since the field is at its maximum when the electrons are stopped at the limits of their motion and vanishes when the electrons are at their maximum velocity, the energy of the system simply oscillates back and forth between field energy and kinetic energy. In metals, the electron density is high and quantum effects are important. Quantized electrostatic oscillations of the conduction electrons in a metal have the energy $E = \hbar\omega$. Other quantum effects are also noticeable. Due to the exclusion principle, the electrons that move into a region that is already filled by other electrons must occupy higher energy levels lying above the Fermi level. This is equivalent, in a sense, to increasing the restoring energy on the electrons, and it has the effect of increasing the frequency. The kinetic energy of free electrons is described approximately by the dispersion relation [10]

$$E_L = \sqrt{\frac{3}{5} \frac{\hbar^2}{m_e} (3\pi^2 n_e)^{1/3} k} \qquad (35)$$

where *k* is the wave number of free electrons. In metals, where the conduction band is only partially filled, the Fermi level lies somewhere in the middle of the conduction band, far from a band edge and the effective mass is very nearly that of a free electron. Figure 6 shows the band structure of the electron energy in a periodic lattice. The broken lines indicate the

dispersion relation of free electrons.
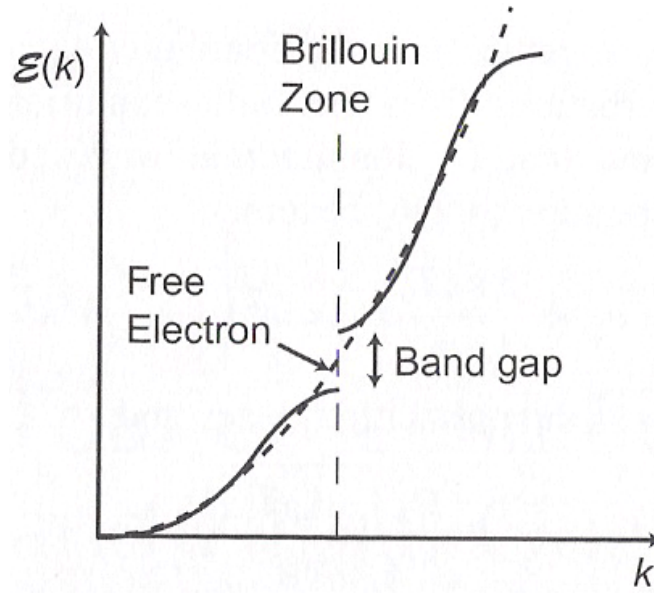
Fig. 6   Band structure of the electron energy in a periodic lattice [10]

The wave number is a critical parameter which is closely related to the self-resonant frequency of polygonal spiral inductors. In this model, the concept of standing wave is implemented to characterize the free electron behavior while the inductor starts self-resonating. The free electrons similar to the notion of standing waves move back and forth through the terminals of the spiral inductor. Thus, the wave number, k, of the electron could be identified as $m\pi/l_{max}$ where m represents an integral number. Once the free electrons behave like standing waves, they can effectively absorb the energy of the EM wave propagating along the inductor. Meanwhile, since the operational frequency falls in a range of 1 to 20GHz for most of RFICs in which the EM wavelength is about centimeters long, the lowest mode would be the dominant one. In other words, the integral number m is equal to unity and $k \sim \pi/l_{max}$. Thus, the self resonant frequency of a spiral inductor would be equal to the frequency of the resonating electron and could be calculated as the following:

$$E_L = \sqrt{\frac{3}{5} \frac{\hbar^2}{m_e} (3\pi^2 n_e)^{1/3} \frac{\pi}{l_{total}}}$$

(36)

For the most part, the hypothesis simply embodies the culmination of the analytic model.

3.3 Scattering Field and Energy Stored in a corner of a spiral inductor

Another assumption is made to facilitate a mental visualization of the electron behaviors inside the polygonal spiral inductor while EM wave propagates along with the entity. Homologizing the hydromechanics that expounds the ideals about the inner corner flow, it can be hypothesized that small free vortexes would locally form in the apex of corner while electrons travel inside the polygonal spiral inductor. Since the vortex is a closed path and its diameter is much smaller than the inductor width, it is convenient to assume that the vortex is infinitesimal in this model. The electrons moving in a form of free vortex can be treated as a cluster of static electrons to build up a quasi-static electric field in the apex of the corner. Thus, according to Jackson's field theory [11] and the notion of hydromechanics, there will be electric fields built up in the neighborhood of corners while an external electric field is applied on a conducting material. To a polygonal spiral inductor with several corners in the boundary, the quasi-static electric field built up in each corner has the form as the following which is calculated by the variation principle [14]

$$\vec{E}(r) = \frac{1}{4\pi\varepsilon_0} \frac{q\left[\pi + 8\sin\left(\pi^2/4\beta\right)\right]^2}{8\beta\varpi \; h\left[\csc(\beta/2) - 1\right](\pi + \beta)} \hat{r} \tag{37}$$

where q is elementary charge, ϖ and h are the width and height of polygon spiral inductor respectively, β is the corner angle, and the field is centered at the outer apex of each corner. By considering the field scattering, free electrons move near the corner would be scattered and alter their trajectories due to the built-up electrical field in the corner. The energy free electrons suffer in the corners due to the field scattering can be calculated as [15, 16]:

$$E_C = \frac{\pi\varepsilon_0\varpi \; h\left[\csc(\beta/2) - 1\right]|\vec{E}|q}{NV^{2/3}\sqrt{\sigma_{eff}}} \left[\left(1 + 2V^{\frac{2}{3}}\int_{-\infty}^{\infty}\frac{dr}{r^3} + ...\right)\csc\left(\frac{\pi - \beta}{2}\right)\right]^2$$

$$= \begin{cases} \dfrac{q^2}{4NV^{2/3}\sqrt{\sigma_{eff}}} \dfrac{\left(\pi + 8\sin\dfrac{\pi^2}{4\beta}\right)^2}{8\beta(\pi + \beta)} \csc^2\left(\dfrac{\pi - \beta}{2}\right), & \text{for } \beta < \pi \\[4mm] \dfrac{q^2}{4NV^{2/3}\sqrt{\sigma_{eff}}} \dfrac{\left(\pi + 4\sqrt{2}\right)^2}{4\pi} \dfrac{\pi}{2.7}, & \text{for } \beta = \pi \text{ (circular inductor)} \end{cases} \tag{38}$$

where N, V, and σ_{eff} are the number of corners, the volume of polygon spiral inductor, and the effective cross section of the inductor, respectively. Here, the effective cross sections are equal to 0.101, 0.281, [17] and 0.375 times the cross section of rectangular, octagonal, and circular inductors, respectively. In above formula, the term

$$1 + 2V^{\frac{2}{3}} \int_{-\infty}^{\infty} \frac{dr}{r^3} + \ldots \ldots \tag{39}$$

means the trajectory function with the perturbation terms. The first term means the ideal trajectory function, and the second terms means perturbation from the near field such as the ground pad, etc. Since we assume the perturbations from the field is far from the infinity, the integral arguments are as the presentation. The recent investigations reveal that the substrate coupling effects could be neglected as long as the air gap is larger than 60μm [18]. For a micromachined inductor in the RFIC design, the reference ground point would be far away from itself. Thus, infinity assumption is reasonable and practical in the model. Nevertheless, if a reference ground plane is designed to close to the inductor, the SRF would be changed and can be calculated in (39) by changing the integral range $[r_m, \infty)$ to replace $(-\infty, \infty)$, where the factor r_m presents a reference point for an inductor circuit. This factor indicates the loss or shift term for applying energy. We will discuss the factor r_m in later chapter in details.

3.4 Energy Conservation and determination of Self-resonant Frequency

Since the built-up electric field near the corners could modify the forward direction of the free electrons and make them move straightly down to the end of the inductor to form the standing waves, the realistic Self-resonant frequency, ω_r, of a polygonal spiral inductor in this model should be derived as the following:

$$\omega_r = \left(E_L + N \cdot E_C\right)/\hbar \tag{40}$$

Equation (40) indicates that the inductor starts resonating to form a standing wave as long as its energy is equal to the electronic kinetic energy plus the total energy stored in the corner.

Chapter 4   Determination of Inductance

4.1   Conventional Methods

In electrostatics we found that the forces on conductors and the energy in the electric field can be described in terms of the charges on the conductors and a set of constants called the capacitance. We are also familiar with the idea that the energy in the magnetic field surrounding a single conductor can be described in terms of the current and a parameter we call the inductance. In this section we address the conventional method which generalizes the notion of inductor with its own current. Then we can computer the total energy in the magnetic field.

It is found that the magnetic field possesses an energy density in a medium

$$u = \frac{1}{2} \vec{B} \cdot \vec{H}^*$$
(41)

In terms of the vector potential, the total energy field is

$$w = \frac{1}{2} \int \left(\nabla \times \vec{A} \right) \cdot \vec{H}^* \, d^3\vec{r} = \frac{1}{2} \sum_{i,j,k=1}^{3} \varepsilon_{ijk} \int H_k \frac{\partial A_j}{\partial r_i} d^3\vec{r}$$
(42)

Taking integrate once by part, we obtain

$$w = \frac{1}{2} \sum_{i,j,k=1}^{3} \varepsilon_{ijk} \left[\int H_k A_j d^2 r_{l\neq i} \Big|_{r_i=-\infty}^{r_i=\infty} - \int A_j \frac{\partial H_k}{\partial r_i} d^3\vec{r} \right]$$
(43)

Since the first term must vanish because of the magnetic field vanishes at infinite, we are left with

$$w = \frac{1}{2} \sum_{i,j,k=1}^{3} \varepsilon_{ijk} \int \frac{\partial H_k}{\partial r_i} A_j d^3\vec{r}$$
(44)

Clearly, the mutual and self-inductance can be given by the formula

$$\frac{1}{2} \sum_{i,j,k=1}^{3} \varepsilon_{ijk} \int \frac{\partial H_k}{\partial r_i} A_j d^3\vec{r} = \frac{1}{2} \sum_{m,n} I_m I_n L_{mn}$$
(45)

where the quantity $L_{mn} = L_{nm}$ is called the mutual inductance for $m \neq n$, and called the

self-inductance for $m = n$.

It is noted that for a closed current-carrying circuit with arbitrary shape such as a spiral inductor the Ampère's law will be annullable from the asymmetry of the shape. There are three independent ways can be employed to overcome the drawback at present. One is using the Biot and Savart law to execute the integrand along the circuit path of the spiral inductor. The integral of current and coordinate function, however, is too complicated to be completed. Other way is to decompose the circuit path into several segments and estimate each one and then sum over all of them. This way may be better than the Biot and Savart law, but the accuracy will be lost seriously. The final way is based on the Greenhouse algorithm. Though the algorithm is very accurate, it still employs numerous summation steps that depend on the number of interacting segments and overall combinations of parallel segments. Complicated geometrical analysis can not be avoided. Meanwhile, there are nonphysical expressions, obtained using a large number of fitting factors. Since the factors are created to overcome the imperfect of the fitting function, it is essential to create an accurate mathematical expression associated with the physical sense for the inductance calculation. In order to break though this predicament, this model poses a simple method to accurately estimate the inductance and self-resonant frequency of an inductor without complicated geometrical analysis and integrand. In addition, the inductance is a function of material parameter, so designer can modify the inductor circuit intuitively and rely on their physical sense to predict the performance of the inductor. A flow chart shown in Figure 7 presents the step to optimize the inductor model.
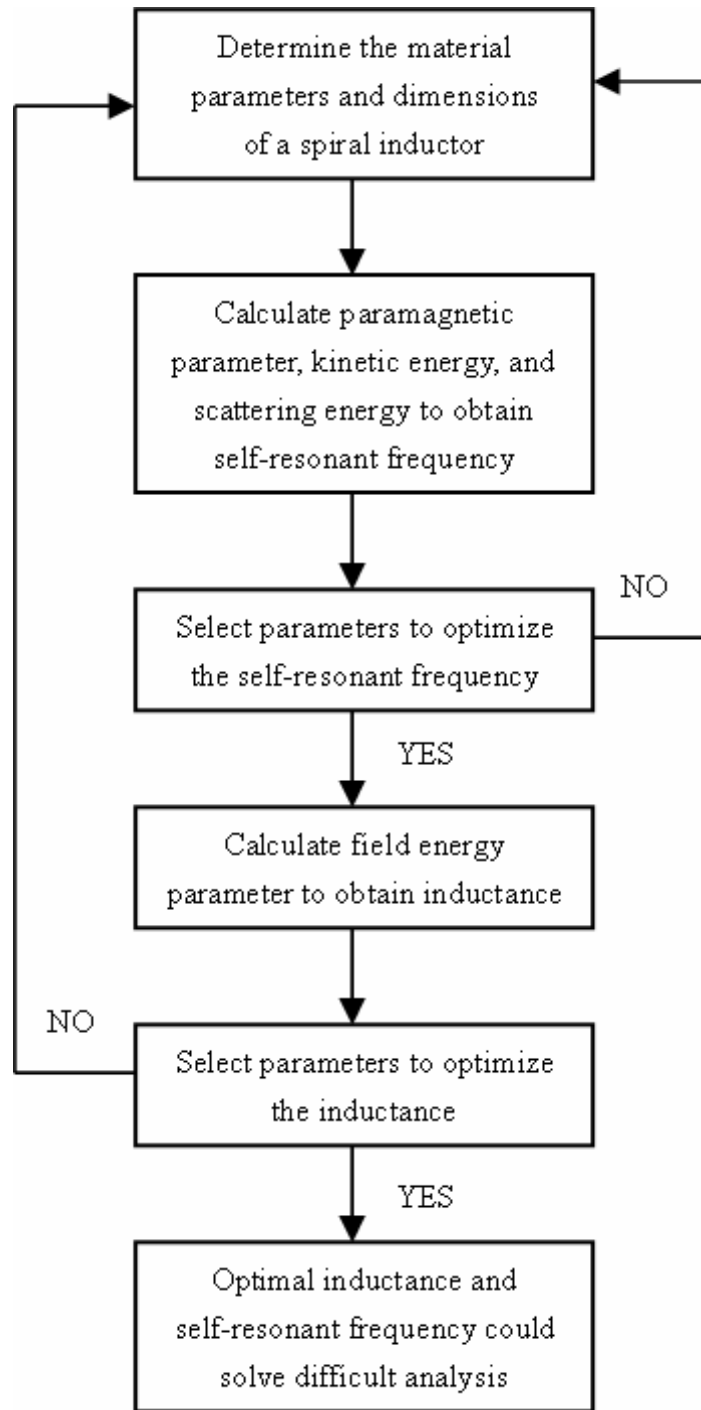
Fig. 7   A flow chart presents the step to optimize the inductor model

4.2 To Determine the Inductance in Solid-State Physics View

In Drude's time, and for many years thereafter, it seems reasonable to assume that the free electronic velocity distribution was given in equilibrium at temperature *T* by the Maxwell -Boltzmann distribution. However, by the advent of the quantum theory and the recognition that for electrons the Pauli Exclusion Principle requires the replacement of the Maxwell-Boltzmann distribution with the Fermi-Dirac distribution. In this model, it is necessary to develop the distribution of the free electrons inside the metals by the modern physical statistics. Thus, the transport behavior of the free electrons should be discussed.

The classical theory of transport processes is based on the Boltzmann transport equation. By working in the six-dimensional space of Cartesian coordinates $\vec{r}$ and velocity $\vec{v}$, the classical distribution function $f(\vec{r},\vec{v})$ is defined by the relation:

$$f(\vec{r},\vec{v})\,d\vec{r}\,d\vec{v} = \text{number of particles in } d\vec{r}\,d\vec{v} \tag{46}$$

The boltzmann equation is derived by the following argument. We consider the effect of a time displacement *dt* on the distribution function. The Liouville theorem of classical mechanics provides a physical model that following a volume element along a flow-line the distribution is conserved:

$$f(t+dt,\vec{r}+d\vec{r},v+d\vec{v}) = f(t,\vec{r},\vec{v}) \tag{47}$$

in the absence of collisions. With collisions

$$f(t+dt,\vec{r}+d\vec{r},v+d\vec{v}) - f(t,\vec{r},\vec{v}) = dt\left(\frac{\partial f}{\partial t}\right)_{\text{collisions}} \tag{48}$$

Thus, the Boltzmann transport equation can be calculated as

$$\frac{\partial f}{\partial t} + \vec{v}\cdot\nabla_{\vec{r}}f + \frac{d\vec{v}}{dt}\cdot\nabla_{\vec{v}}f = \left(\frac{\partial f}{\partial t}\right)_{\text{collisions}} \tag{49}$$

In many problems the collision term may be treated by the introduction of a relaxation time $\tau(\vec{r},\vec{v})$, defined by the equation

$$\left(\frac{\partial f}{\partial t}\right)_{\text{collisions}} = -\frac{(f-f_0)}{\tau} \tag{50}$$

where f_0 is the energy distribution function in thermal equilibrium. Thus, this result provides a way to address the distribution of free electron density with magnetic energy in the complex frequency plane, defined as

$$f_0(\omega) = \frac{n_e \hbar \omega_r}{2\pi} \left[\exp\left(\frac{\hbar(\omega - \omega_r)}{k_B T} \right) + 1 \right]^{-1} \tag{51}$$

By the normalization condition and integral the magnetic energy function, we obtain the total magnetic energy:

$$F(\omega) = \left| \frac{1}{n} \int f_0(\omega) d^3 \vec{r} \right| = \frac{n_e l_{total} h \varpi \, \hbar \omega_r}{2\pi \, n} \left[\exp\left(\frac{\hbar(\omega - \omega_r)}{k_B T} \right) \right]^{-1} \tag{52}$$

Shortly after the discovery that the Pauli Exclusion Principle was needed to account for the bound electronic states of atoms, Sommerfeld applied the same principle to the free electron gas of metals, and thereby resolved the most flagrant thermal anomalies of the early Drude model. In most applications Sommerfeld's model is nothing more than Drude's classical electron gas with the single modification that the electronic velocity distribution is taken to be the quantum Fermi-Dirac distribution rather than the classical Maxwell-Boltzmann distribution. Figure 8 shows the Maxwell-Boltzmann and Fermi-Dirac distributions for typical metallic densities at room temperature, in which both curves are for the density given by $T = 0.01 T_0$. The scale is the same for both distributions, and has been normalized so that the Fermi-Dirac distribution approaches 1 at low energies. It is noted that the Maxwell-Boltzmann distribution will close to infinity while the electron gas is in the ground state and violate the underlying physical phenomenon for electrons. Thus, it is necessary and reasonable to employ the Fermi-Dirac distribution rather than the Maxwell-Boltzmann distribution in this model.

After all, by extracting the susceptibility function, magnetic factor, and self-resonant frequency in chapter 3 and employing the conception of the velocity distribution from Sommerfeld's theorem in which Fermi-Dirac distribution was adopted, the inductance of a rectangular micromachined spiral inductor can be derived with the associated magnetic energy of EM field in the inductor:
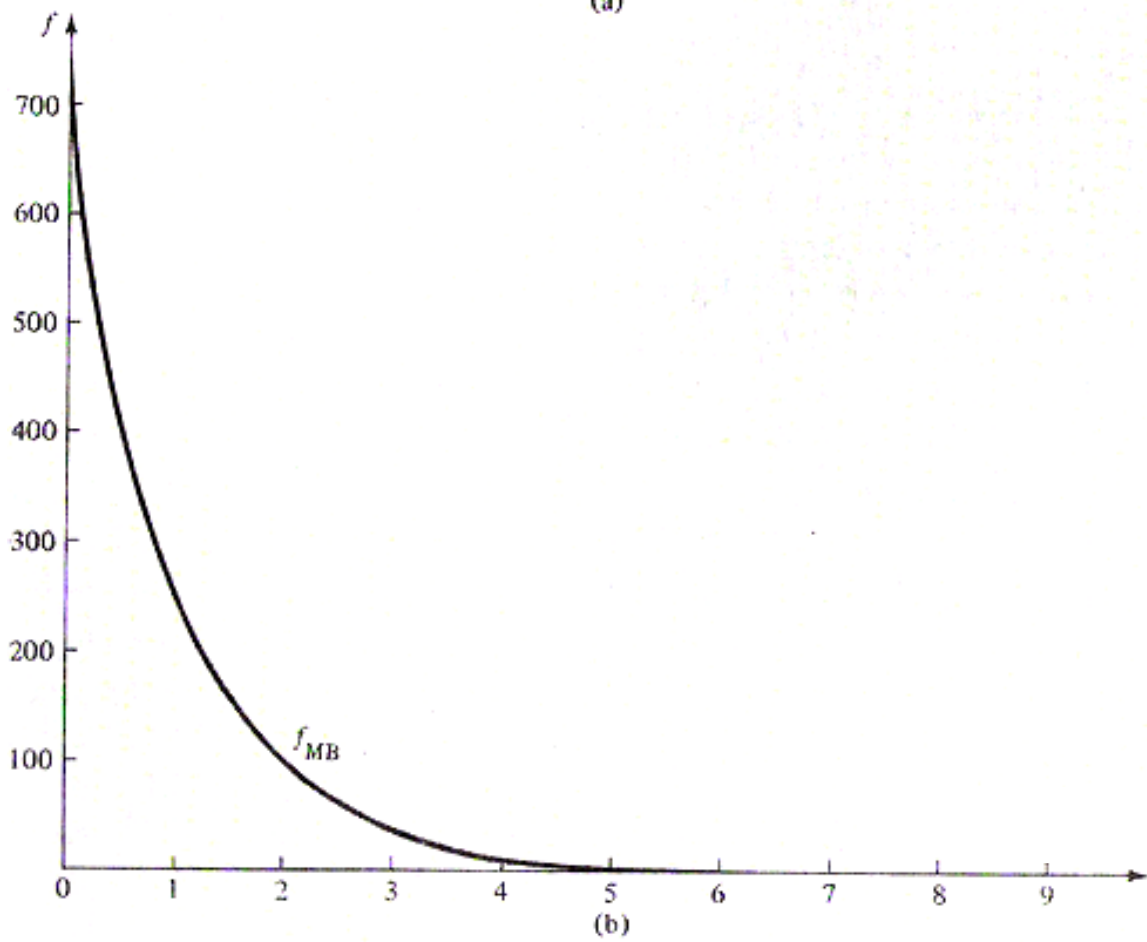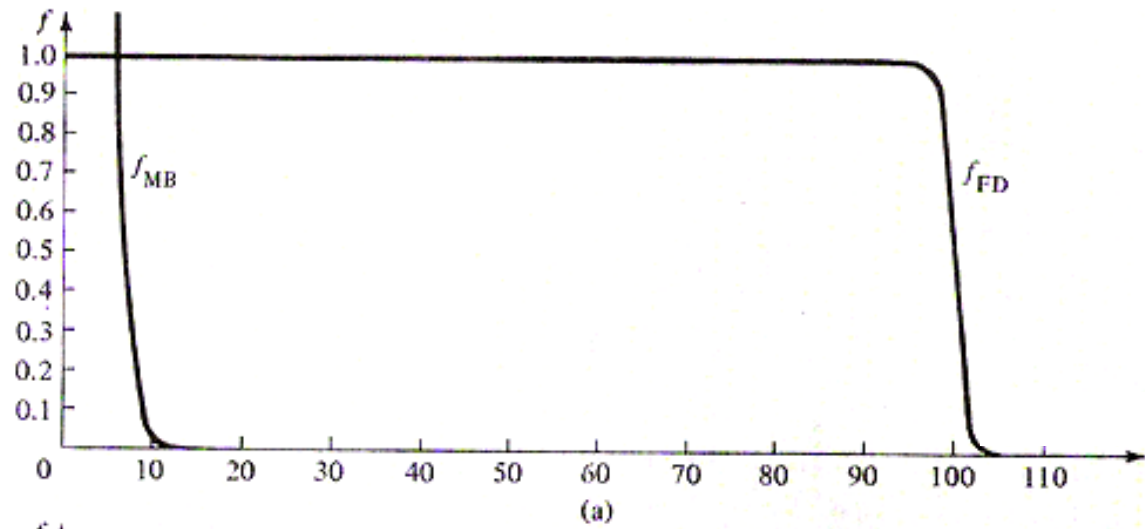
Fig. 8   Maxwell-Boltzmann and Fermi-Dirac distributions for typical metallic densities at room temperature, in which both curves are for the density given by $T = 0.01T_0$ [13]

$$L_{\rm rec} \equiv \frac{\int \vec{B} \cdot \vec{H}^* d^3\vec{r}}{I^2}$$

$$\cong \frac{\mu_0 \chi F(\omega)}{\left(\sigma_0 \dfrac{h\varpi}{l_{total}}\right)^2} = \mu_0 \frac{n_e l_{total}^3 \chi \hbar \omega_r}{2\pi\sigma_0^2 An} \left[\exp\left(\frac{\hbar(\omega - \omega_r)}{k_B T}\right) + 1\right]^{-1} \qquad (53)$$

where A, k_B and T are the cross section area ($= h\varpi$), the Boltzmann's costant, and absolute temperature, respectively.

Similarly, the inductance of octagonal and circular spiral inductor can also be estimated respectively as

$$L_{\rm oct} \approx \mu_0 \frac{3n_e l_{total}^3 \chi \hbar \omega_r}{5\pi\sigma_0^2 An} \left[\exp\left(\frac{\hbar(\omega - \omega_r)}{k_B T}\right) + 1\right]^{-1} \qquad (54)$$

and

$$L_{\rm cir} \approx \mu_0 \frac{n_e l_{total}^3 \chi \hbar \omega_r}{\pi\sigma_0^2 An} \left[\exp\left(\frac{\hbar(\omega - \omega_r)}{k_B T}\right) + 1\right]^{-1} \qquad (55)$$

In the equation (53), (54) and (55), the free electron density and conductivity indicated that the inductance shall depend on the characteristics of material and the dimension of the inductors seriously. The susceptibility function also addresses that the difference of the magnetic properties.

It is noted that the conductivity is actually frequency-dependent (or is called AC conductivity) and is given by

$$\sigma(\omega) = \frac{\sigma_0}{1 - i\omega\tau} \qquad (56)$$

where τ is the relaxation time of a free electron. Fortunately, the order of the relaxation time of a free electron for typical metals is about 10^{-24} second, so that the denominator can be seen as unity even though the self-resonant frequency of the inductors is approached. Thus, DC conductivity employed in equation (53), (54) and (55) is reasonable and practical.

Chapter 5   Ground Pad Issue

5.1   Spherical Green's function expansion and electric energy

In order to pose the issue of interaction from ground pad to the interesting system, to develop a proper Green's function is actually necessary, in which the Dirichlet condition is employed to describe the special situation at boundary surface. Electric energy is adopted to estimate the influence of direction from the ground pad to the spiral inductor edge side. In this section, a special solution of electric energy will be developed. The general solution to the Poisson equation with specified values of the potential on the boundary surface by using Dirichlet condition is:

$$\Phi(\vec{x}) = \frac{1}{4\pi\varepsilon_0} \int_V \rho(\vec{x}') G(\vec{x},\vec{x}') d^3x' - \frac{1}{4\pi} \oint_S \Phi(\vec{x}') \frac{\partial G}{\partial n'} da' \tag{57}$$

where the expansion of the Green's function for a spherical shell bounded by $r = a$ and $r = b$ is:

$$G(\vec{x},\vec{x}') = 4\pi \sum_{l=0}^{\infty} \sum_{m=-l}^{l} \frac{Y_{lm}^*(\theta',\phi') Y_{lm}(\theta,\phi)}{(2l+1)\left[1-\left(\frac{a}{b}\right)^{2l+1}\right]} \left(r_<^l - \frac{a^{2l+1}}{r_<^{l+1}}\right) \left(\frac{1}{r_>^{l+1}} - \frac{r_>^l}{b^{2l+1}}\right) \tag{58}$$

As a preliminary, the region we are interested in is between the radius of $r = a$ and $r = b$. We now turn the attention to the solution of problems with charge distributed in the volume, so that the volume integral in equation (57) is involved. It is necessary to consider problems in which the potential vanishes on the boundary surfaces in many applications. By linear superposition of a solution of the Laplace equation, the general situation can be obtained. The first consideration is that of a hollow grounded sphere of radius b with a concentric ring with charge of radius a and total charge Q. The ring of charge is located in the x-y plane, as shown in Figure 9. The charge density of the ring can be written with the help of delta functions in angle and radius as
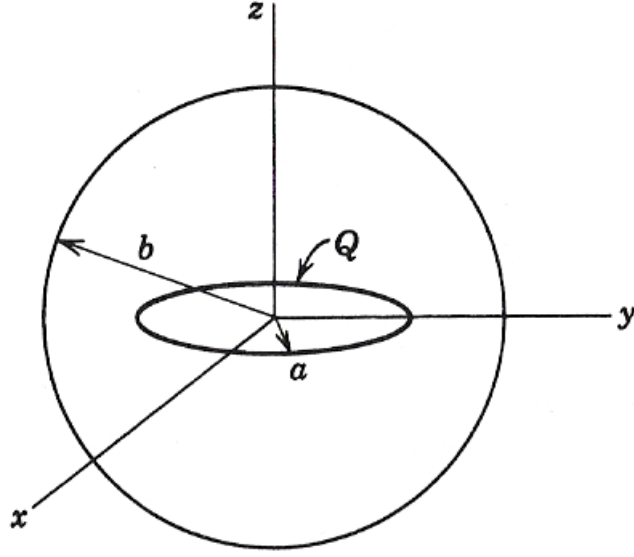
Fig. 9   The ring of charge is located in the x-y plane [11]

$$\rho(\vec{x}') = \frac{Q}{2\pi a^2} \delta(r' - a)\delta(\cos\theta') \tag{59}$$

In the volume integral over the Green's function only terms in equation (56) with $m = 0$ will survive because of azimuthal symmetry. Then the potential expansion becomes

$$\Phi(\vec{x}) = \frac{1}{4\pi\varepsilon_0} \int_V \rho(\vec{x}') G(\vec{x}, \vec{x}') d^3 x'$$

$$= \frac{Q}{4\pi\varepsilon_0} \sum_{n=0}^{\infty} \frac{(-1)^n (2n-1)!!}{2^n n! \left[1 - \left(\frac{a}{b}\right)^{4n+1}\right]} \left(r_<^{2n} - \frac{a^{4n+1}}{r_<^{2n+1}}\right) \left(\frac{1}{r_>^{2n+1}} - \frac{r_>^{2n}}{b^{4n+1}}\right) P_{2n}(\cos\theta) \tag{60}$$

where $r_< = \min(r,a)$ and $r_> = \max(r,a)$. In order to simplify the problem, we can first reduce the equation (58) as:

$$\Phi(\vec{x}) = \sum_{n=0}^{\infty} T_n \left(\frac{1}{r_>^{2n+1}} - \frac{r_>^{2n}}{b^{4n+1}}\right) P_{2n}(\cos\theta) \tag{61}$$

where

$$T_n = \frac{Q}{4\pi\varepsilon_0} \frac{(-1)^n (2n-1)!!}{2^n n! \left[1 - \left(\frac{a}{b}\right)^{4n+1}\right]} \left(r_<^{2n} - \frac{a^{4n+1}}{r_<^{2n+1}}\right) \tag{62}$$

29

Since the interesting space is between the ranges of radius a to b on the x-y plane, we may obtain the radial electric field by taking the differentiation of the potential respect to $r_>$ and take $\theta = \dfrac{\pi}{2}$. Thus, we get the radial electric energy as:

$$
\begin{aligned}
\left. E_r \right|_{\theta=\frac{\pi}{2}} &= -\frac{1}{r_>^2}\frac{\partial}{\partial r_>}\left(r_>^2 \Phi\right)\Bigg|_{\theta=\frac{\pi}{2}} = \sum_{n=0}^{\infty} T_n\left[\frac{2n-1}{r_>^{2n+2}}+\frac{(2n+2)r_>^{2n-1}}{b^{4n+1}}\right]P_{2n}(0) \\
&= \sum_{n=0}^{\infty} T_n'\left[\frac{2n-1}{r_>^{2n+2}}+\frac{(2n+2)r_>^{2n-1}}{b^{4n+1}}\right]
\end{aligned}
\tag{63}
$$

where

$$
T_n' = \frac{Q}{4\pi\varepsilon_0}\left(\frac{(-1)^n(2n-1)!!}{2^n n!}\right)^2 \frac{r_<^{2n}-\dfrac{a^{4n+1}}{r_<^{2n+1}}}{1-\left(\dfrac{a}{b}\right)^{4n+1}}
\tag{64}
$$

Therefore, we can evaluate the specific electric energy related to the boundary and system (here the word "system" can be posed as a spiral inductor later) in which $a \to 0$ is adopted to simplify the problem and the form is:

$$
\begin{aligned}
\mathrm{E} &= \frac{\varepsilon_0}{2}\left|E_r\right|^2 \\
&= \frac{\varepsilon_0}{2}\sum_{n=0}^{\infty}\sum_{m=0}^{\infty} B_m B_n r_<^{2m+2n}\left[\frac{2n-1}{r_>^{2n+2}}+\frac{(2n+2)r_>^{2n-1}}{b^{4n+1}}\right]\left[\frac{2m-1}{r_>^{2m+2}}+\frac{(2n+2)r_>^{2m-1}}{b^{4m+1}}\right]
\end{aligned}
\tag{65}
$$

where

$$
B_x = \frac{Q}{4\pi\varepsilon_0}\left(\frac{(-1)^x(2x-1)!!}{2^x x!}\right)^2 , \quad x = m,n
\tag{66}
$$

30

5.2 Modification of trajectory function

Both conceptually and physically, the interaction from the ground pad to the interesting system such as a spiral inductor will rely on the electric energy decreasing associated with the direction between them. In most engineering applications the ground pad of an on-chip circuit may closely surround with the system, and then the influences form the ground pad can not be ignored. In this case we can slightly discuss the ground pad issue now by altering the conditions, such as b = distance from the origin to the ground pad edge, $r_<$ = distance from the origin to the innermost edge of the spiral inductor, and $r_>$ = distance from the origin to the outermost edge of the spiral inductor in the equation (65) and (66). Thus, by comparing the equation (38) and (65) with the terms of $m = 0$ and $m = 1$, we can obtain the relation:

$$\left| 2\int \frac{dr}{r^3} \right| V^{\frac{2}{3}} = \frac{1}{r_m^2} V^{\frac{2}{3}} = \frac{2r_<^2 r_>}{b^5} V^{\frac{2}{3}} \tag{67}$$

However, in some real cases the relation (67) can not provide correct results because of the difference of the mathematical structure of the Green's Function. The relation constructed by the spherical Green's function generally can not completely describe the behaviors of electric fields within the device structure with arbitrary shape of inductors and ground pad but that of circular ones. Thus, it is necessary that to construct a general coordinate Green's function with the Dirichlet condition to describe the field behaviors in any shape of the device structures. Unfortunately, it is very difficult to develop the seriously mathematical and physical structures of the general coordinate Green's function. In the drawback like this situation, an approximate method to estimate the filed behaviors will help us to understand somewhere the operations of the fields within the structure.

Taking 5μm thick micromachined copper rectangular spiral inductors with restricting their geometric factors as l_{max} = 300μm, S = 5μm, and ϖ = 15μm as examples, Figure 10 will show the relations between equation (67) and relative error percentage of self-resonant frequency calculated by equation (36), (38) and (40). The details will not be discussed here because of the mathematical tools still can not undertake the requirements of the physical
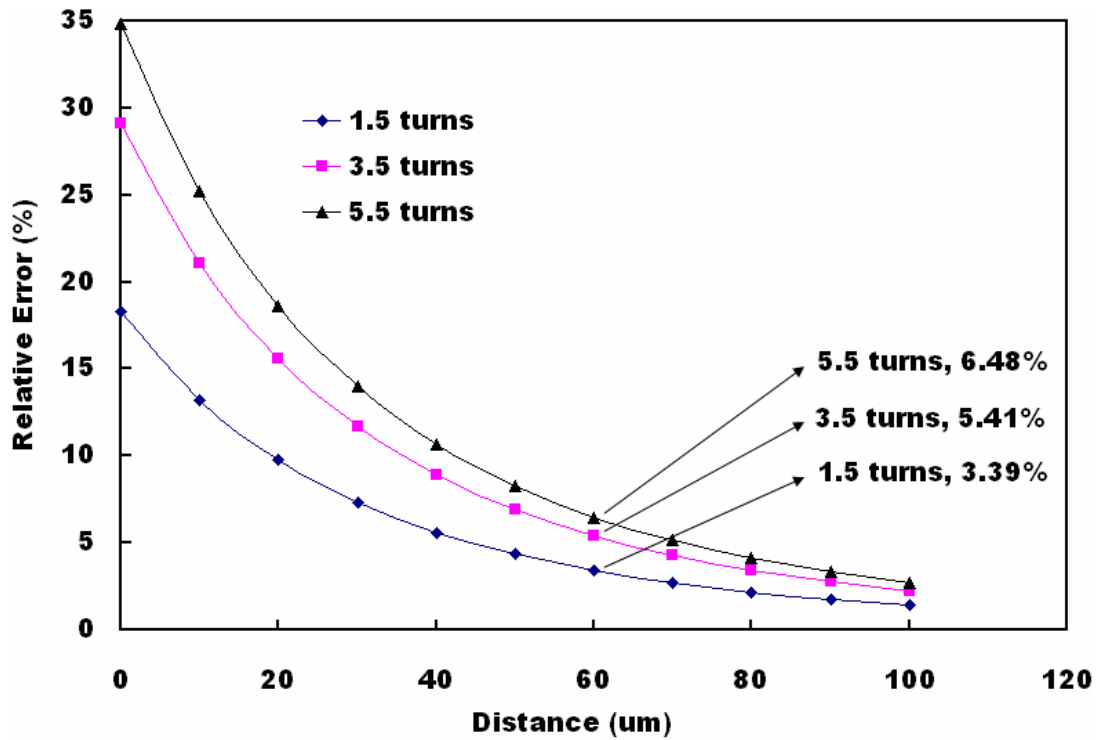
problems.

Fig. 10   Relations between distance from inductor edge to ground pad and relative error of self-resonant frequency

As presented in the presented study [18], the result of model calculation poses the fact that the inductor can be seen as a freely system while the ground pad far from 60 μm at least. Thus, the spherical Green's function can tell us the approximate results without any confusion. In the future, the general coordinate Green's function should be developed to resolve the more complicated physical and mathematical problems.

Chapter 6   Model Validation and Discussion

6.1 Model Validation

So far, we have developed the Kramers-Kronig relations for metal in order to character the behaviors of free electrons while the anomalous absorption occurring. The kinetic energy and scattering potential of the free electrons inside the spiral inductors were calculated to achieve the prediction of the self-resonant frequency of the inductors. The hypothesis of the magnetic energy density was posed to estimate the inductance of the rectangular, octagonal and circular spiral inductors. Finally, the ground pad issue was slightly discussed. Therefore, all of the significant overcomes will be addressed in this chapter.

Considering the fabricated structure of a 5μm thick and 3.5 turns micromachined copper spiral inductor with restricting its geometric factors as $l_{max}= 300$μm, $S = 5$μm, and $\varpi = 15$μm, as shown in Figure 11. It is noted that the rectangular spiral inductor is freely-suspend on the air gap. The substrate effect will be avoided in order to simplify the inductor model. Thus, the further work and simulations will follow this simplification in this chapter. By adding the suitable boundary condition, wave port excitation, and the ground pad consisted of perfect conductor, the 3-D structures of rectangular, octagonal, and circular spiral inductors with substrate removal were built and simulated, and as shown in Figure 12, 13, and 14, respectively.

In the Ansoft-HFSS simulator, the radiation boundary condition presents the surface that the electromagnetic wave can pass through from the region of the existence of the device to the outer region but in the opposite direction. The default boundary, however, means that the electromagnetic wave may be reflected from the external region and enter the inner region. The excitation of the simulation is defined by adding semi-infinite long wave guides, wave ports and impedance lines, which are pointed from the ground pad to one side of the wave port, on the two terminals of the spiral inductors. The employing wave guides are consisted of perfect conductors in which the skin effect may not be considered, thus the propagated

electric and magnetic fields are perpendicular to the surface of the strip. In addition, the whole device is included into box, as shown associated with Fig 12, 13, and 14 in the right-down corners, in which the radiation boundary condition is adopted and is filling by air.

In general, it is difficult but important to construct the step of the port-source and boundary condition for the micromachined inductors. Experimentally, the distance between the boundary condition and the center of inductor was set up as twelve times of the dimension of inductor. In addition, the ground-signal-ground pads, as shown in Figure 12, were attached to the terminals of inductor as measured pads. The scale of two square wave ports is about eight times of the width of signal pads [19]. The results of modeling extracted from Ansoft-HSFF simulator will be de-embedded on the S-parameters.
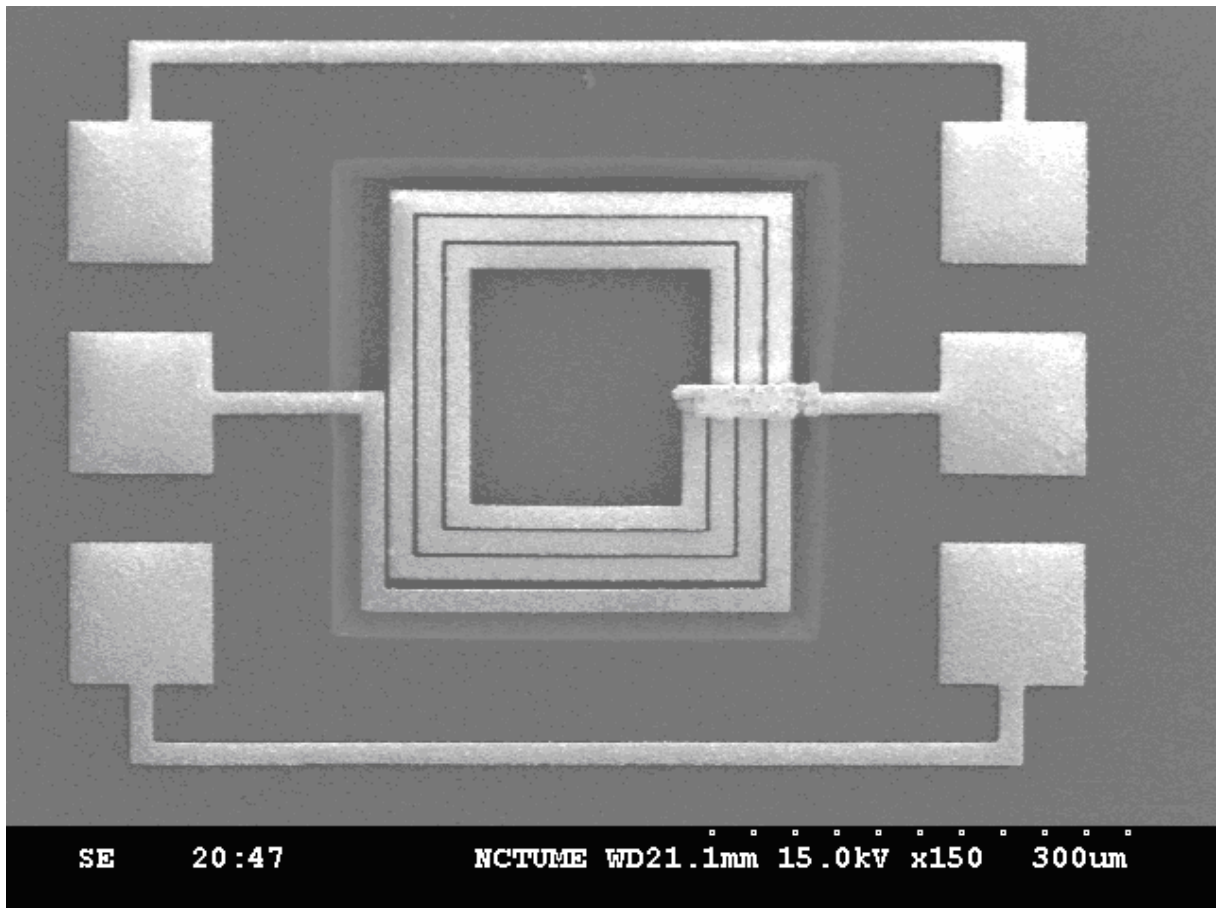

Fig. 11   Scheme of a freely suspend micromachined rectangular spiral inductor with restricting its geometric factors as $l_{max} = 300\mu m$, $S = 5\mu m$, and $\varpi = 15\mu m$.
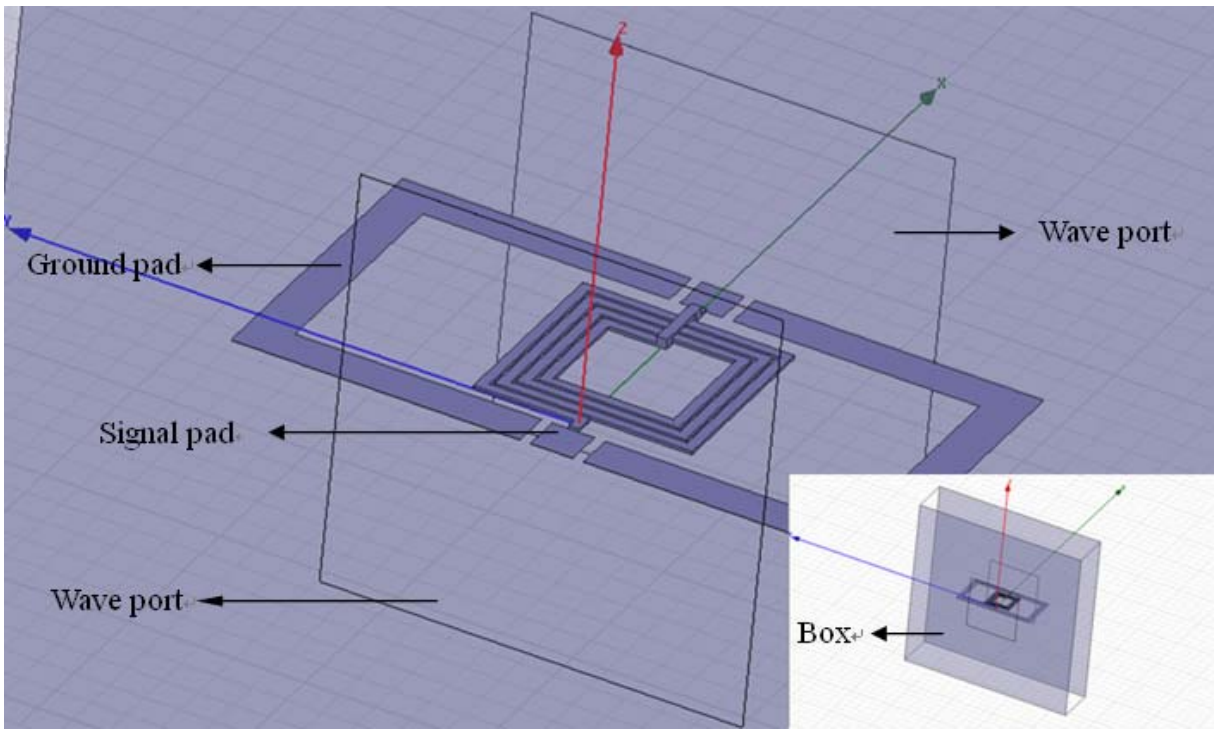
Fig. 12　　Scheme of rectangular spiral inductor with substrate removal
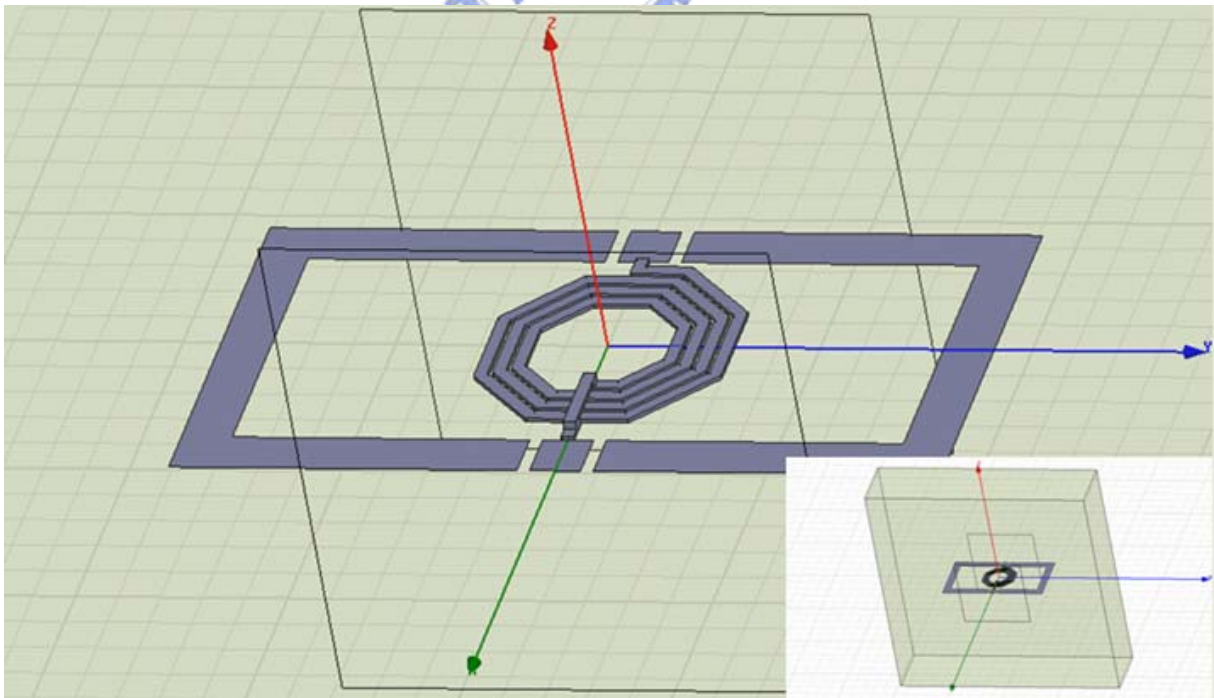

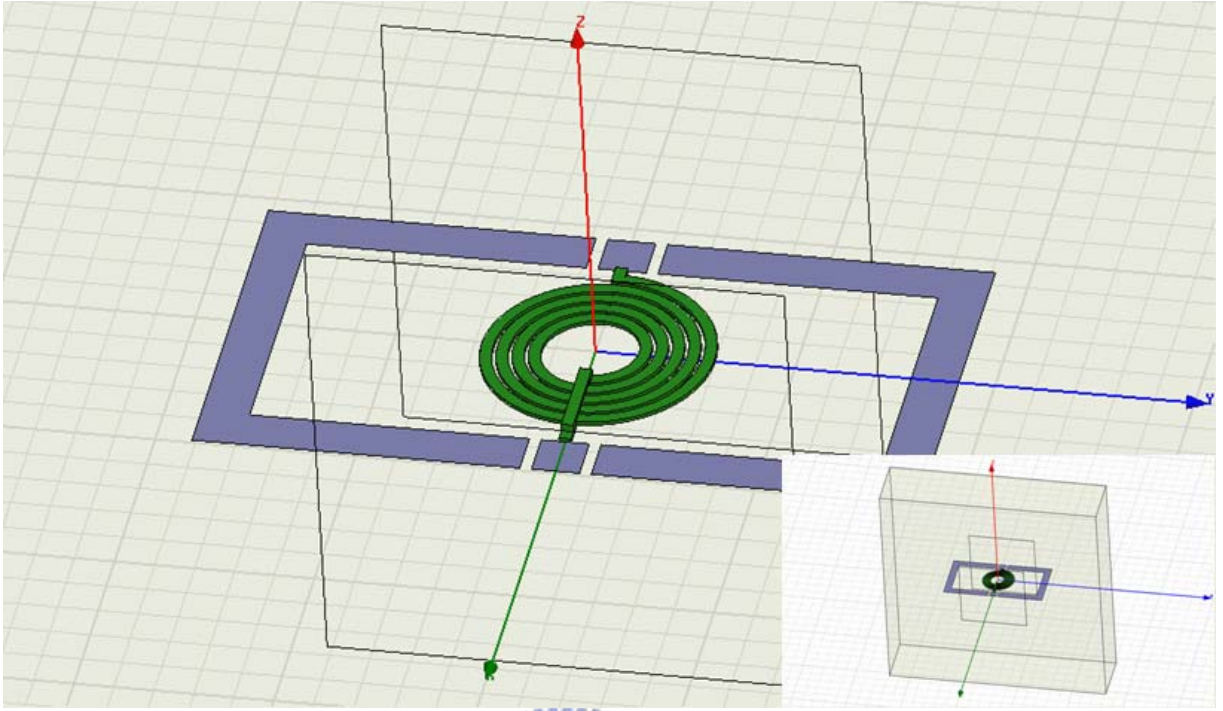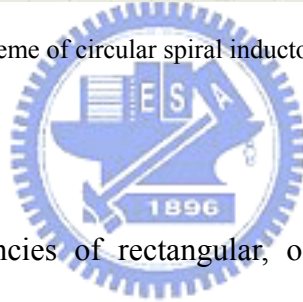Fig. 13　　Scheme of octagonal spiral inductor with substrate removal.

Fig. 14　　　Scheme of circular spiral inductor with substrate removal.

The self-resonant frequencies of rectangular, octagonal, circular inductors could be predicted well by means of utilizing the equation (34), (36), (38), and (40), and the values are shown in Table 1. Then, we could determine the required inductances at particular frequency by the equation (53) for rectangular spiral inductor and the values are shown as in Table 2. In table 1 and 2, we will see that our model is examined by comparing with the contemporary calculations including the results derived from Greenhouse based model [2] and Ansoft-HFSS simulator, respectively. A good S-parameter match between the measurement and HFSS simulation in a Smith chart which is shown in Figure 15 presents the fact that the accuracy of the HFSS analysis is experimentally validated in the Table 1 and 2. It is noted that Greenhouse based model does not provide the frequency dependence of the inductance. The symbol, X, used in Table 2 means it does not be available. The material utilized here is copper with the properties of $n_e = 8.45 \times 10^{28} \, \mathrm{m}^{-3}$, $m_e = 9.11 \times 10^{-31} \, \mathrm{kg}$, and $\sigma_0 = 5.6 \times 10^7 \, (\mathrm{m}\Omega)^{-1}$.

TABLE 1

SELF-RESONANT FREQUENCY WITH DIFFERENT TYPE OF INDUCTORS

Comparisons (n=3.5)	Self-resonant frequency based on our model (GHz)	Self-resonant frequency based on HFSS (GHz)
Rectangular inductor	23.9	22.9
Octagonal inductor	24.9	23.6
Circular inductor	25.8	24.6

TABLE 2

COMPARISON RESULTS OF RECTANGULAR SPIRAL INDUCTORS

| Number of Turns Comparisons (n)	1.5	2.5	3.5	4.5	5.5
ω_r for HFSS (GHz)	39.5	27.1	22.9	20.6	19.4
ω_r for K. K. model (GHz)	38.6	28.6	23.9	21.4	19.9
ω_r for Greenhouse (GHz) based model	X	X	X	X	X
L for HFSS @ 3GHz (nH)	1.58	2.94	4.27	5.31	6.01
L for K. K. model @ 3GHz (nH)	1.18	2.65	4.13	5.32	5.95
L for Greenhouse based model @ 3GHz (nH)	1.60	3.02	4.28	5.18	5.60
L for HFSS @ 5GHz (nH)	1.58	2.99	4.38	5.49	6.21
L for K. K. model @ 5GHz (nH)	1.19	2.71	4.25	5.51	6.20
L for HFSS @ 9GHz (nH)	1.63	3.22	4.92	6.31	7.23
L for K. K. model @ 9GHz (nH)	1.24	2.91	4.74	6.33	7.30
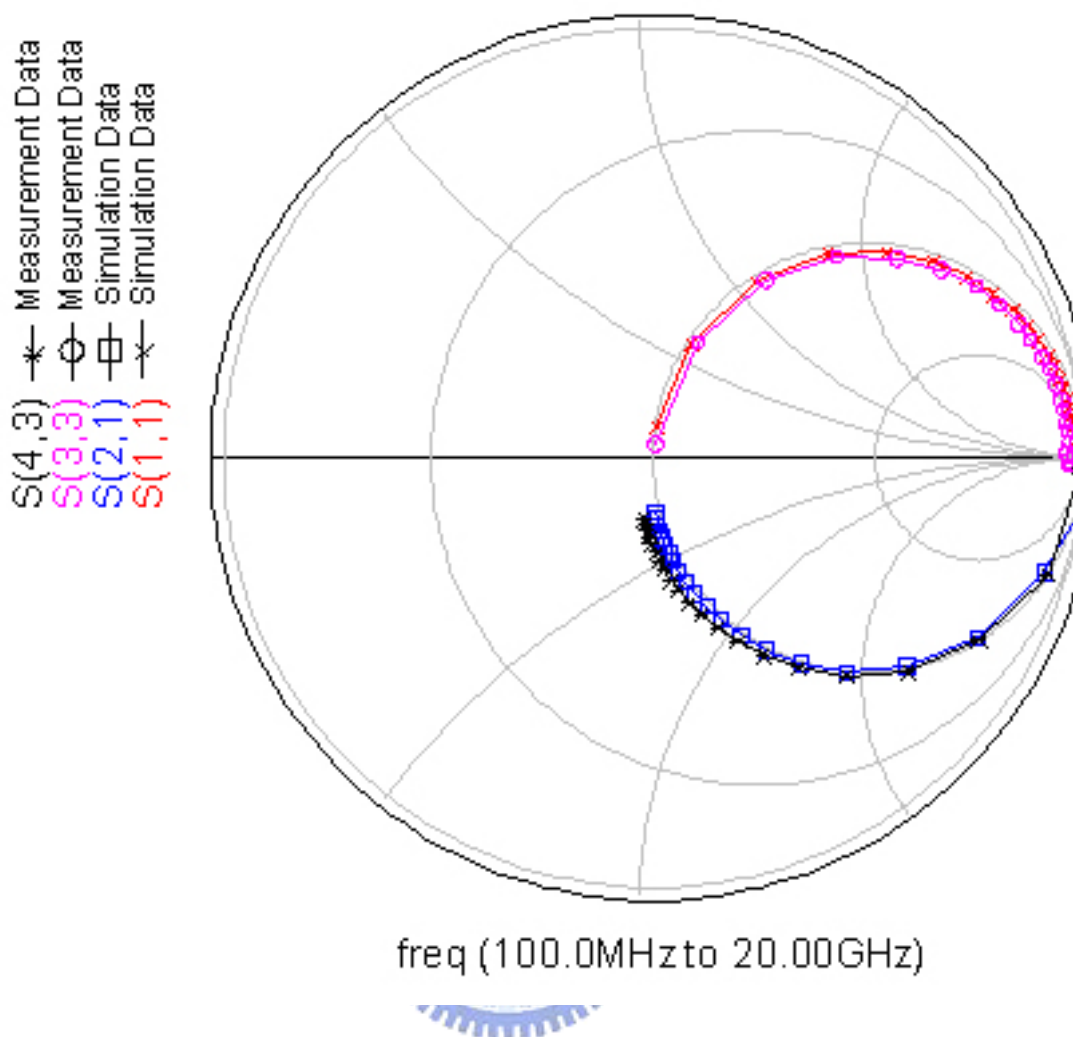
Fig. 15   Smith chart in which a good s-parameter match between measurement and simulation is present.

The inductance expression based on this model is closely fitted with the simulation and experimental data for the structure of the spiral inductor with substrate removal. The above table also indicated that not alike our model the greenhouse model does not provide the self-resonant frequency itself and can not determine the inductances associated with the frequency change. The comparison of inductance spectrum is shown as Figure 16.

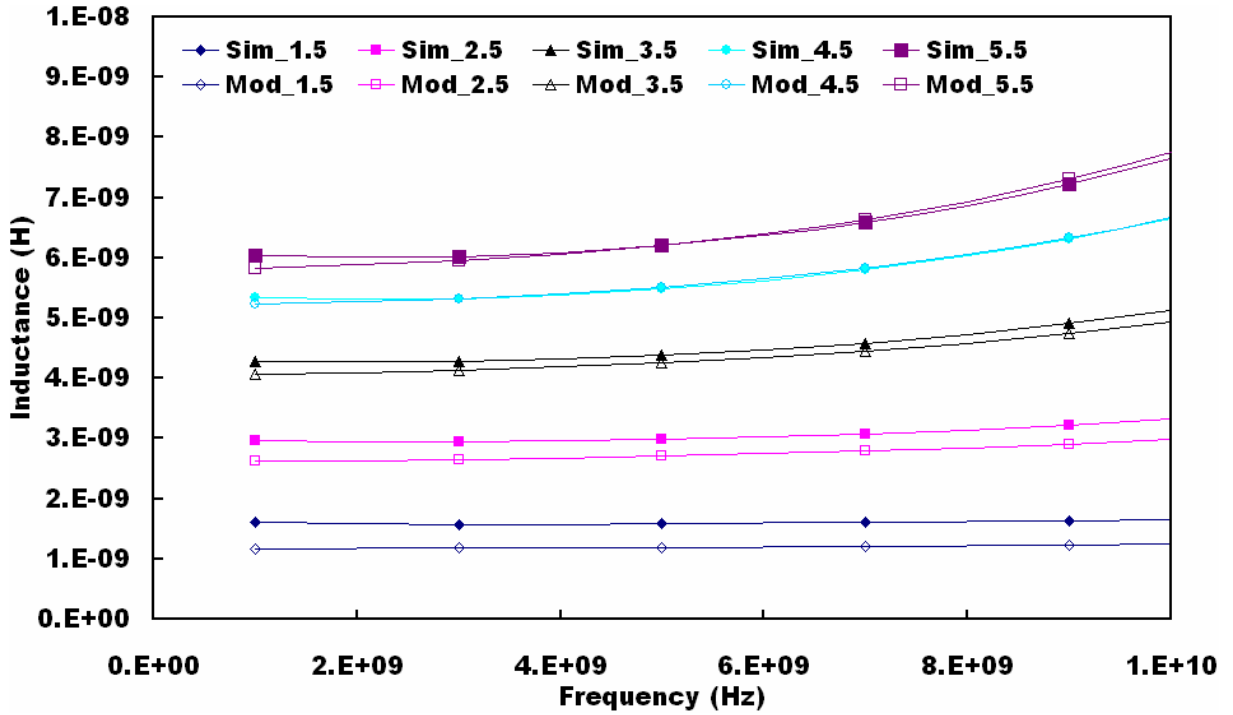Fig. 16   Comparison of inductance spectrum of rectangular spiral inductors and results of simulation

Utilizing similar boundary conditions, the comparison of octagonal and circular spiral inductors between inductance extracted from the simulator and equation (54) and (55) are shown in Figure 17 and 18, respectively.
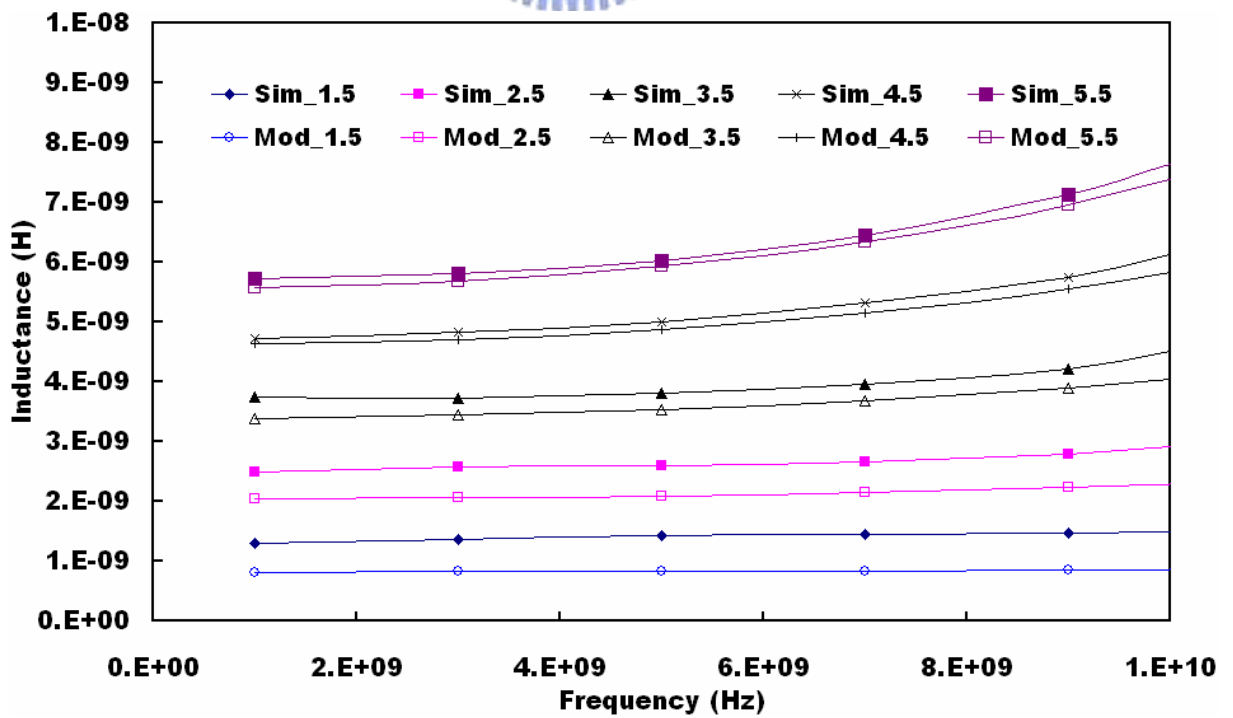

Fig. 17   Comparison of inductance spectrum of octagonal spiral inductors and results of simulation
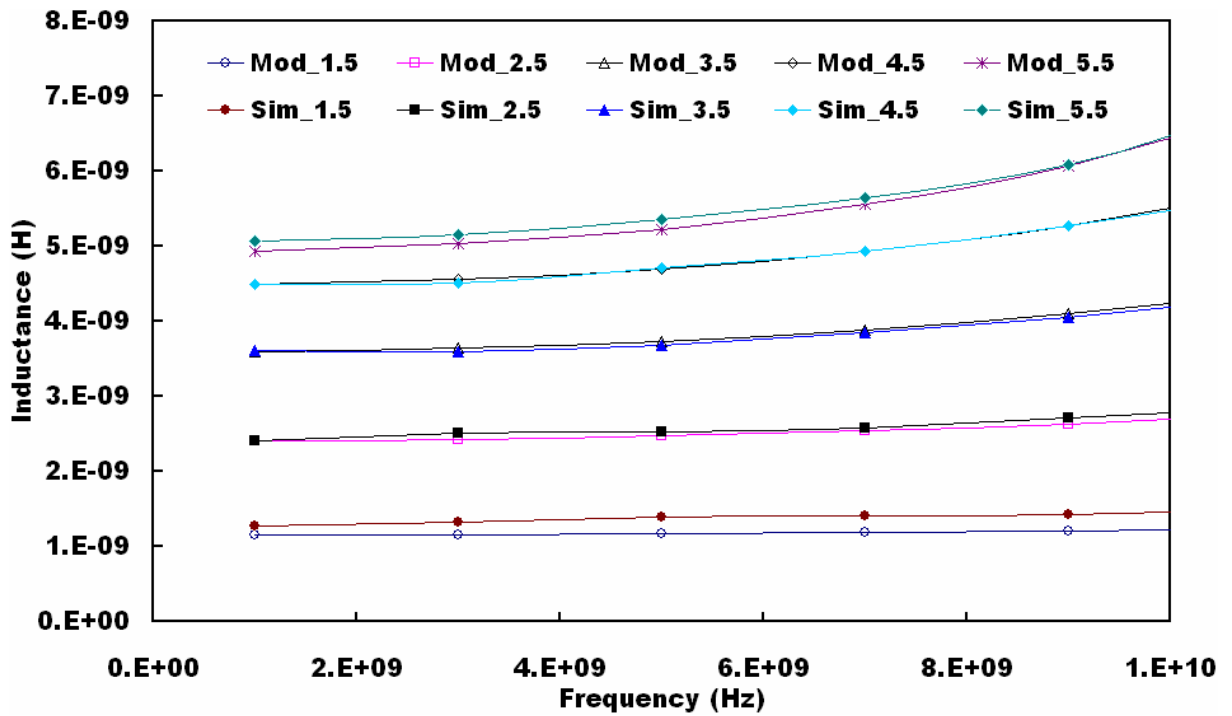
Fig. 18   Comparison of inductance spectrum of circular spiral inductors and results of simulation

Note that again this inductor model could predict the self-resonant frequency and inductance of a on-chip freely spiral inductor and the designer could easily satisfy their requirements by means of modifying the geometry and material parameters of their inductor circuit. The analytical method based on Kramers-Kronig relations, EM field theory and solid state physics could provide us mathematically convenience for the inductor design in physical senses.

6.2 Discussion and Future Work

A premise must be emphasized again that the physical model are constructed with substrate removal for the simplification. Since the substrate coupling effect is not included in this model at this moment, the micromachined type inductor is the best test vehicle to examine this model. In comparison with the other calculations as listed in Table 2, this closed-form integral model can provide a very closely prediction with less than 2% relative deviation. Besides, it also reveals the relations between the inductor characteristics and the geometry factors and material properties of inductor. The physical parameters will allow us to optimize the inductor design. At present, the integral can only well simulate the behaviors of micromachined inductor and has its potential applications for the design of high performance RFICs due to the high quality characteristic of the inductor [20, 21]. However, we think that the integral can be further modified for general on-chip inductors by considering the affections of magnetic factor and self-resonant frequency resulted by substrate coupling effect.

In addition, based on the Boltzmann transport equation and the principle of least action, the universe formulations of prediction of self-resonant frequency and inductance might be searched out to match the nature principle of physics. Thus, the energy lose into the substrate can be only treated as a frequency-depended operator associated with geometrical and material parameters in the modeling prediction. By deeply exploring the underlying physical meaning of the Pauli spin paramagnetism at "room" temperature and the carefully calculating the energy perturbation near the Fermi surface, the physical model can have more widely utilization and compatibility of materials. Furthermore, this closed-form physical model can also potentially be utilized to modify the characteristics of spiral inductors which are constructed by nanocomposite materials. The self-resonant frequency and inductance can be exactly determined by means of the superposition of susceptibility functions of inductor itself and the nano-fillers and the geometrical parameters.

In the future, other characteristics of the on-chip inductor, such as qualify factor, energy

loss mechanics, parasitic capacitors, parasitic resistors must be developed and discussed in details. We hope that a Smith chart constructed by this model with strongly physical senses will be presented to achieve the goals of optimized designs.

Reference

[1] H. M. Greenhouse, "Design of planar rectangular microelectronic inductor," <u>IEEE Trans. Parts, Hybrids, Packag.</u>, vol. PHP-10, no. 2, pp. 101–109, Jun. 1974.

[2] S. Jenei, B. K. J. C. Nauwelaers, and S. Decoutere, "Physics-based closed-form inductance expression for compact modeling of integrated spiral inductors," <u>IEEE J. Solid-State Circuits</u>, vol. 37, no. 1, pp. 77–80, Jan. 2002.

[3] S. Asgaran, "New accurate physics-based closed-form expressions for compact modeling and design of on-chip spiral inductors," in Proc. 14th Int. Conf. Microelectronics, Dec. 2002, pp. 247–250.

[4] S. S. Mohan, M. M. Hershenson, S. P. Boyd, and T. H. Lee, "Simple accurate expressions for planar spiral inductance," <u>IEEE J. Solid-State Circuits</u>, vol. 34, no. 10, pp. 1419–1424, Oct. 1999.

[5] A. M. Niknejad and R. G. Meyer, <u>Design, Simulation and Applications of Inductors and Transformers for Si RF ICs</u>. Boston, MA: Kluwer, 2000.

[6] S. S. Mohan, M. M. Hershenson, S. P. Boyd, and T. H. Lee, "Simple accurate expressions for planar spiral inductance," <u>IEEE J. Solid-State Circuits</u>, vol. 34, no. 10, pp. 1419–1424, Oct. 1999.

[7] Y. Koutsoyannopoulos et al., "A generic CAD model for arbitrary shaped and multilayer integrated inductors on silicon substrates," in Proc. ESSDERC'97, 1997, pp. 320–323.

[8] J. R. Long and M. A. Copeland, "The modeling, characterization and designed monolithic inductors for silicon RF ICs," <u>IEEE J. Solid-State Circuits</u>, vol. 32, no. 3, pp. 357–369, Mar. 1997.

[9] A. M. Niknejad and R. G. Meyer, "Analysis, design and optimization of spiral inductors and transformers for Si RF ICs," <u>IEEE J. Solid-State Circuits</u>, vol. 33, no. 10, pp. 1470–1481, Oct. 1998.

[10] C. A. Brau, <u>Modern Problems in Classical Electrodynamics</u>. New York: Oxford Univ., 2004.

[11] J. D. Jackson, <u>Classical Electrodynamics</u>. 3rd New York: Wiley, 1998.

[12] C. Kittel, <u>Introduction to Solid State Physics</u>, 7th Ed. New York:Wiley, 2004.

[13] N. W. Ashcroft and N. D. Mermin, Solid State Physics. New York: Holt-Sanders, 1976.

[14] G. B. Arfken and H. J. Weber, <u>Mathematical Methods for Physicists</u>, HP, 2001.

[15] A. S. Kronfeld and B. Nižić, "Nucleon Compton scattering in perturbative QCD," <u>Physics Review D</u>, vol. 44, pp. 3445-3465, 1991.

[16] F. J. Federspiel, R. A. Eisenstein, M. A. Lucas, B. E. MacGibbon, K. Mellondorf, A. M. Nathan, A. O'Neill, and D. P. Wells, "Proton Compton effect: A measurement of the electric and magnetic polarizabilities of the proton," <u>Physics Review Letters</u>, vol. 67, pp. 1511-1514, 1991.

[17] C. C. Chen, J. K. Huang, and Y. T. Cheng, "A Closed-Form Integral Model of Spiral Inductor Using the Kramers–Kronig Relations," <u>IEEE Microwave and Wireless Components Letters</u>, vol. 15, pp. 778-780, 2005.

[18] J. Y. Park and M. G. Allen, "High Q spiral-type microinductors on silicon substrates," <u>IEEE Transactions on Magnetics</u>, vol. 35, no. 5, pp. 3544-3546, 1999.

[19] Manual of Ansoft HFSS, *conf.* NCHC, R. O. C.

[20] H. Lakdawala, X. Zhu, X, H. Luo, S. Santhanam, L. R. Carley, and G. K. Fedder, "Micromachined high-Q inductors in a 0.18-μm copper interconnect low-k dielectric CMOS process", <u>IEEE, JSSC</u>, pp. 394-403, 2002.

[21] J. Hongrui, Y. Wang; J. –L. A. Yeh, and N.C Tien, "On-chip spiral inductors suspended over deep copper-lined cavities" <u>IEEE Microwave Theory and Techniques</u>, pp. 2415-2423, 2000.

Vita and Publications

姓　　名：陳健章(Chien-Chang Chen)

出生日期：中華民國七十年十二月十八日

出 生 地：中華民國花蓮縣

聯絡電話**(Mobile phone)**：0928-847300

電子郵件信箱**(E-mail address)**：gettgod.ee92g@nctu.edu.tw

學 經 歷**(Education & Experience)**：

1996.7. ~~ 1999.6.：國立花蓮高中 (National Hen-Lian Senior High School)

1999.7. ~~ 2003.6.：國立中央大學物理學系學士

(Department of Physics, National Central University)

2003.7. ~~ 2006.6.：國立交通大學電子工程學系電子研究所碩士

(Department of Electronics Engineering & Institute of Electronics,

National Chiao-Tung University)

發表著作**(Publication)**：

1. Jr-Wei Lin, C. C. Chen, J. K. Huang, and Y. T. Cheng, "An optimum design of the micromachined RF inductor," *IEEE Radio Frequency Integrated Circuits (RFIC) Symposium*, pp. 639-642, Fort Worth TX, 6-8 June 2004.

2. Jr-Wei Lin, C. C. Chen, and Yu-Ting Cheng, "A robust high-Q micromachined RF inductor for RFIC applications," *IEEE Transactions on Electron Devices*, pp. 1489-1496, Vol. 52, 2005.

3. C. C. Chen, J. K. Huang, and Y. T. Cheng, "A closed-form integral model of spiral inductor using the Kramers-Kronig relations," *IEEE Microwave and Wireless Components Letters*, pp.778-780, Vol. 15, 2005.